Florida State University Libraries

Electronic Theses, Treatises and Dissertations The Graduate School

2006

Modeling of Solid Oxide Fuel Cell/Gas Turbine Hybrid Systems

Nischal Srivastava

Follow this and additional works at the FSU Digital Library. For more information, please contact lib-ir@fsu.edu

THE FLORIDA STATE UNIVERSITY
FAMU-FSU COLLEGE OF ENGINEERING

MODELING OF SOLID OXIDE FUEL CELL / GAS TURBINE HYBRID SYSTEMS

By

NISCHAL SRIVASTAVA

A Thesis submitted to the
Department of Mechanical Engineering
in partial fulfillment of the
requirements for the degree of
Master of Science

Degree Awarded:
Summer Semester, 2006

The members of the Committee approve the thesis of Nischal Srivastava defended on 07-07-2006.

_____
Juan C. Ordonez
Professor Directing Thesis

_____
Peter McLaren
Committee Member

_____
Cesar Luongo
Committee Member

Approved:

_____
Chiang Shih, Chair, Department of Mechanical Engineering

_____
Ching-Jen Chen, Dean, FAMU-FSU College of Engineering

The Office of Graduate Studies has verified and approved the above named committee members.

TABLE OF CONTENTS

LIST OF TABLES

LIST OF FIGURES

ABSTRACT

There is a growing interest in fuel cells for hybrid system. Fuel cells when combined with conventional turbine power plants offer high fuel efficiencies. The feature of certain fuel cells (SOFC, MCFC), which makes them suitable for hybrid systems, is their high operating temperature. In this work, a detailed thermodynamic model of SOFC/Gas turbine hybrid system is simulated in Matlab-Simulink. Various configurations of the hybrid configuration are proposed and analyzed. A comparative study based upon performance parameters, such as SOFC power, turbine inlet temperature, and exhaust temperature is used to select the best configuration. Simple thermodynamic models for the compressor and turbine are used during the configuration selection. Once the configuration is selected, more realistic compressor and turbine models based on performance maps are incorporated into the model and used to study design and off-design performance of the hybrid system. The results are compared to the available literature.

1. INTRODUCTION

1.1 BACKGROUND

The idea of energy conversion can be considered to be as old as the history of humankind on the earth. It goes back to thousands of years back when humans were learning to understand the concept of energy. From Middle Pleistocene humans' idea of controlling fire (by burning wood) in 500,000 BC to the use of coal by northeastern Chinese to smelt copper in 1000 BC to the current state of technology such as fuel cells or photovoltaic cells, humankind has continuously tried to tap the potential of energy for his better [Equest, 2006]. When we look back how this development has taken shape, we come across many situations when all the focus was to make the things work irrespective of its effects on the society. Perhaps it is a common trend of any development path that we invent new things first and then try to improve them. But now as we see when development of technology spans over thousands of years and we know many novel ways of extracting energy, attention is focused not only on production of energy but also on its quality. The idea is still more or less the same as to extract the maximum possible from the resources available but there are some other important things such as sustainability of energy, its affect on the environment and on the coming generations to name a few that have come to our attention and seem to have a great importance in the current energy scenario.

1.2 CURRENT ENERGY SCENARIO

The developing approach towards energy production is based upon the guiding principles "consume less, generate more" tied to other important aspects: environment friendliness, affordability and sustainability. So far the energy production has largely depended upon the fossil fuels, which are still a major source of energy. Besides the limited capacity of fossil fuels and their direct affect on living species caused by emissions, there are other reasons (such as increasing percentage of CO_2, SO_2 and other compounds which disturb the natural environmental equilibrium causing large weather changes), which motivate current research to look for alternative way of energy production.

The hydrogen economy focuses on the production of energy from hydrogen, which is the most abundant element on earth, with minimum environmental impact. One of the technologies that fit into the concept of the hydrogen economy is the fuel cell. This work focuses on solid oxide fuel cells and their synergism with conventional devices of energy production.

1.3 FUEL CELL HISTORY

A fuel cell is a device, which converts chemical energy to electrical and thermal energy by means of an electrochemical process. Since fuel cells are not thermal engines, their efficiency is not set by

the Carnot limit and high energy conversion efficiencies can be achieved compared to traditional power generating devices. This concept of direct energy conversion is not new. In 1838, Sir William Robert Groves, for the first time, combined hydrogen and oxygen electrochemically to produce electricity.

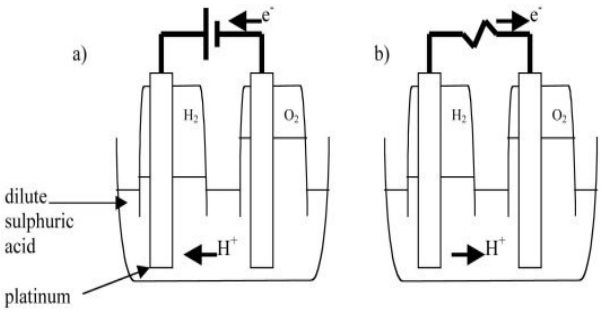

Figure 1-1 Groves Fuels Cell

Grove discovered that a constant current would flow between two platinum electrodes when they are placed with one end immersed in a container of sulfuric acid and the other ends separately sealed in containers of oxygen and hydrogen (Figure 1-1). He noted that the water level rose in both tubes as the current flowed, indicating that the gases reacted. By combining several sets of these electrodes in a series circuit, he created what he called a "Gas Battery"-now known as the fuel cell [Larminie, 2000]. The following reaction gives a better insight of what is happening in the cell:

At the anode of the fuel cell, hydrogen ionizes to give protons and electrons,

$$2H_2 \rightarrow 4H^+ + 4e^- \qquad (1\text{-}1)$$

At the cathode oxygen combines with these electrons to give oxygen ions, hydrogen ions from the anode react with these oxygen ions to produce water,

$$O_2 + 4e^- + 4H^+ \rightarrow 2H_2O \qquad (1\text{-}2)$$

Electrons produced at anode travel to cathode via an external load to produce electricity. The above reactions continue to produce electricity as long as there is a supply of hydrogen and oxygen [Larminie, 2000].

The main problem with Groves' fuel cell was electrode flooding. Though there were several attempts to improve the efficiency of the gas battery and prevent the electrode flooding, it was only in 1889, that Charles Langer and Ludwig Mond created the first prototype of the fuel cell and coined the term Fuel Cell for the Gas Battery. They used a porous non-conducting solid impregnated with an electrolyte which allowed only the movement of hydrogen ions across it. There were further attempts to create a practical fuel cell that could generate electricity from coal but the internal combustion engine swept across all the hope of further development of fuel cell [FCtoday, 2006].

In 1932, Francis Thomas Bacon developed the first successful fuel cell which used Nickel electrodes, a rather inexpensive material as compared to the platinum used by Langer and Ludwig Also, instead of using a sulphuric acid electrolyte, he used potassium hydroxide, which is less corrosive to the electrodes. This fuel cell was the first in a category later known as Alkaline Fuel Cells (AFC). But due to some technical hurdles, it was only twenty seven years later in 1959, that he could produce a truly workable fuel cell of 5 kW capacity enough to power a welding machine. But it soon came into general attention that he was not the only person to produce a workable fuel cell. In the same year, Karl Ihrig, a farm equipment manufacturer, produced a 15 kW fuel cell stack using 1008 fuel cell units enough to power a 20 HP tractor [FCtoday, 2006].

Also in the late 1950s, NASA was looking for a way to power its incoming series of manned space flights. Other options such as nuclear power and solar power were either too risky or too expensive. The only option that seemed lucrative was the fuel cell. NASA granted thousands of research contracts to develop a practical working design for its space mission. Early in the 1960's, the aircraft manufacturing company Pratt & Whitney supplied alkaline fuel cells to NASA for its Apollo space mission and since then AFC's have been integral part of NASA space missions including the Space Shuttle flights [FCtoday, 2006] and [CAPS, 2005].

1.4 FUEL CELL ARCHITECTURE AND THEIR TYPES

A single fuel cell unit generally consists of an anode and a cathode separated by a porous non-conducting electrolyte. The following figure depicts the basic architecture of a fuel cell.

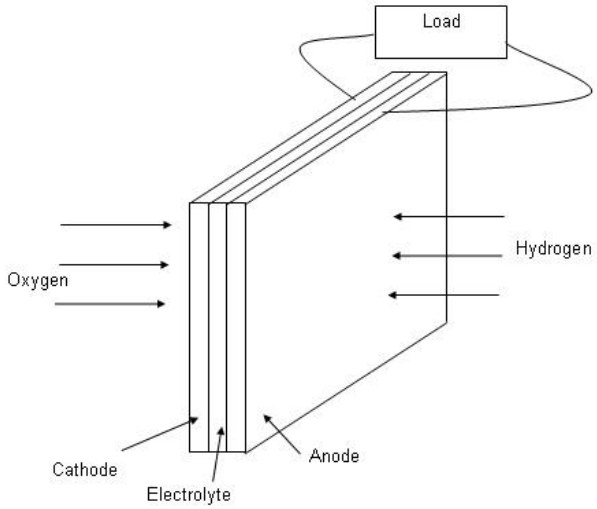

Figure 1-2 Basic Cathode-Electrode-Anode Assembly of a fuel cell unit

Fuel cells are classified by their electrolytes. Common types of fuel cells are polymer electrolyte fuel cells (PEM), phosphoric acid fuel cells (PAFC), alkaline fuel cells (AFC), molten carbonate fuel cells (MCFC) and solid oxide fuel cells (SOFC).

Polymer electrolyte membrane or also known as proton exchange membrane fuel cells (PEM) work in the low temperature range (60-80 ^{0}C) allowing a faster startup of the system. PEM fuel cells are being seen as potentially lucrative for automobile applications because of their high power density and less complex structure as compared to the other fuel cells [FCH, 2004]. Alkaline fuels cells (AFC) as the name suggests use potassium hydroxide as electrolyte. The advent of alkaline fuel cells in 1960 was the beginning of modern fuel cells development. NASA used AFC's for its Apollo space mission and it still continues to use AFC's for onboard power of its space shuttle missions [2, 6]. Phosphoric acid fuel cell (PAFC) was the first commercial fuel cell. The number of units built so far exceeds any other fuel cell technology. The largest power plant of PAFC built to date is 11MW of capacity [C-Doctors, 2006]. Molten carbonate fuel cells (MCFC) and solid oxide fuel cells (SOFC) fall under the high temperature fuel cells category. MCFC operates at around 650 ^{0}C in order to insure the sufficient conductivity of carbonate electrolyte. There are several benefits of high temperature fuel cells over low temperature fuel cells. High operating temperatures eliminates the use of noble metals as catalyst and also, because of the high temperature of the exiting streams, a bottoming cycle can be used to increase the overall system efficiency. Solid oxide fuel cells (SOFC) use a ceramic electrolyte and operate in the 800-1100 ^{0}C temperature range, which makes them suitable for cogeneration [Larmine, 2000].

1.5 SOFC/GAS TURBINE HYBRID SYSTEM

Hybrid systems combine two or more power generating devices and make use of the synergism to generate maximum power and offer higher efficiencies. Hybrid systems typically present low combustion temperature resulting in low exhaust temperature and zero or low level of nitrogen oxides.

The exhaust of a high temperature fuel cell can be expanded in a gas turbine to drive a compressor, which in turn provides pressurized streams to the fuel cell. The residual enthalpy can be used in other turbine stages resulting in additional power.

There are several configurations in which a fuel cell and a gas turbine can be arranged as a cycle. Figure 1-3 shows a particular configuration of a micro GT/SOFC hybrid system. The air stream is pressurized in a compressor and passes through a recuperator where it is preheated. The fuel stream from the pump and the air stream from the recuperator enter the SOFC. Within the fuel cell, fuel and air react electrochemically to generate electricity and a high enthalpy exhaust. This high enthalpy exhaust is mixed with bypassed air stream from the recuperator and combusted in an oxidizer. This high temperature and high pressure effluent is now expanded in the turbine to provide work to drive the compressor and an electrical generator. In this way, the waste heat from the fuel cell is utilized to increase the system efficiency [Samuelsen, 2004].

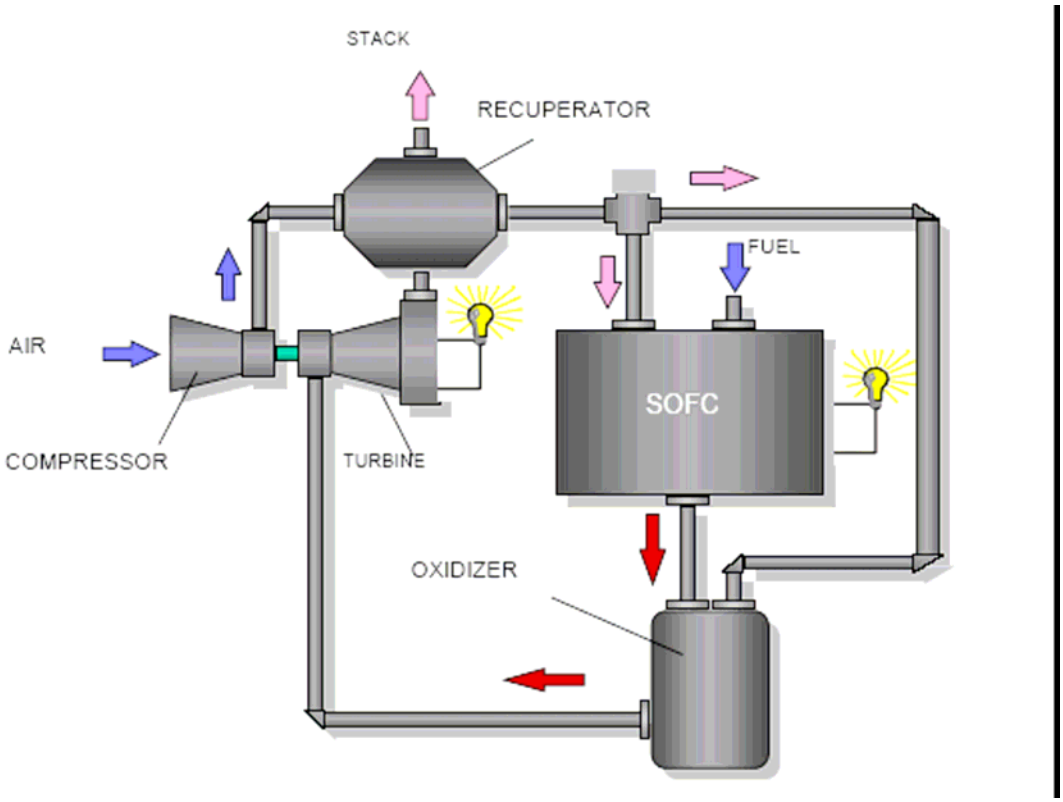

Figure 1-3 MTG-SOFC Hybrid Configuration [Samuelsen, 2004]

1.6 THESIS OUTLINE

This thesis deals with solid oxide fuel cell and gas turbine hybrid systems. It consists of six chapters. Chapter 1 provides a historical perspective of energy and its stages of development. The reader develops an understanding about the suitability of the fuel cells in the current energy scenario. Finally, the chapter offers a historical development of fuel cells, their types and the concept of synergism. Chapter 2 introduces the reader to the electrochemical and thermodynamic fundamentals of the solid oxide fuel cell with its different types and basic characteristics. After that, the chapter presents the concept of bottoming cycle, its main components and their basic operation. A review of current state of art inline with the present work has been dealt in chapter 3. A detailed description of hybrid system component modeling is given in chapter 4. Chapter 5 deals with the hybrid system's optimization and its performance analysis. Concluding remarks and scope of future work have been discussed in chapter 6.

2. TECHNOLOGY OF SOFC/GT HYBRID SYSTEMS

The purpose of this chapter is to introduce the basic concepts and performance issues of solid oxide fuel cells, which are necessary to understand the following chapters and the building blocks of SOFC/GT hybrid systems. These concepts have been taken from various references and are quoted as needed for the interest of the reader.

2.1 SOLID OXIDE FUEL CELL

Solid oxide fuel cells owe their name to their solid electrolyte (zirconia), which is a ceramic and a good conductor of oxygen ions. This property of zirconia was first discovered by Nernst in late 1890's. Though the technology has evolved in these hundred years and production methods have improved, zirconia is still considered to be the best electrolyte for solid oxide fuel cells. Zirconia starts conducting oxygen ions when its temperature is above 700 ^{0}C and thus solid oxide fuel cells are best suited for co-generation purposes. Waste heat from the fuel cell can be utilized in a bottoming cycle and conversions efficiencies of more that 65% are achievable. Also, within the SOFC operating temperature range, emissions of NOx are likely to be very small resulting in a cleaner environment [Larmine, 2000], and [CAPS, 2005].

2.1.1 THERMODYNAMICS AND ELECTRODE KINETICS OF SOFCs

A solid oxide fuel cell can be considered to be an electro chemical reactor which converts hydrogen and oxygen into electricity. Figure 2-1 shows the processes taking place in a solid oxide fuel cell. It basically consists of two porous electrodes (anode and cathode) separated by a ceramic electrolyte, and flow channels for fuel and air delivery and collection.

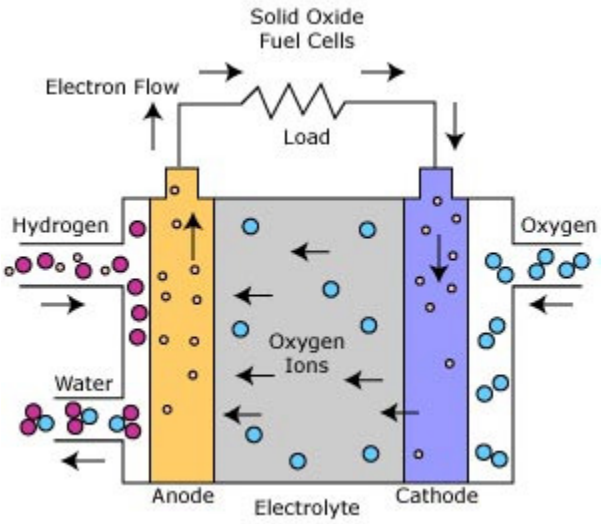

Figure 2-1 Schematic of a Solid Oxide Fuel Cell

H_2 or a hydrocarbon (e.g. methane) is supplied on the anode and air or O_2 on the cathode side of the fuel cell. H_2 and CO (if H_2 is not pure) diffuse through the porous anode to the three phase boundary formed by the anode, the electrolyte and the gaseous H_2. Similarly, O_2 diffuses through cathode to three phase boundary of the cathode side where it accepts electrons from the cathode and gives oxygen ions (Equation 2-1). These oxygen ions travel through the porous electrolyte and react with H_2 to produce electrons and water at the anode (Equation 2-2) and thus an electro motive force is generated between two electrodes. The two electrodes can be connected via an external circuit and an electrical current can be generated [Larmine, 2000].

At the cathode: $$O_2 + 4e^- \rightarrow 2O^{--} \quad (2\text{-}1)$$

At the anode: $$2H_2 + 2O^{--} \rightarrow 4H_2O + 4e^- \quad (2\text{-}2)$$

In cases where CO is present in the H_2 stream, the CO reacts with H_2O via a water gas shift reaction that produces H_2 and CO_2.

Water gas shift at anode:

$$CO + H_2O \leftrightarrow CO_2 + H_2 \quad (2\text{-}3)$$

Before we begin to look at how the electromotive force (EMF) and thus work is produced in a fuel cell, it is necessary to understand some basic thermodynamic concepts [FCH, 2004]. Consider the following thermodynamic identity for a reversible process when there is no shaft work extracted and the system is restricted to do only expansion work:

$$dG = VdP - SdT \quad (2\text{-}4)$$

if the process is isothermal, the above equation reduces to:

$$dG = VdP \quad (2\text{-}5)$$

using the ideal gas relation, $PV=nRT$ in Equation 2-5 where n is the number of moles of the gas, we get

$$dG = nRTdP/P \quad (2\text{-}6)$$

integrating Equation 2-6 from state 1 to state 2, we get,

$$G_2\text{-}G_1 = nRTln(P_2/P_1) \quad (2\text{-}7)$$

If the state 1 is replaced with some standard reference state, with Gibbs free energy G^0 and standard pressure P^0, the Gibbs free energy per unit mole at any state *'i'* is given by,

$$g_i=g^0 + RTln(P_i/P^0) \quad (2\text{-}8)$$

Consider that the following chemical reaction takes place at constant pressure and temperature,

$$aA + bB \leftrightarrow mM + nN \tag{2-9}$$

where *a*, *b, m, and n* are the stoichiometric coefficients of the reactants *A* and *B* and the products *M* and *N*, respectively. Now, Equation 2-8 takes the following form,

$$\Delta G = \Delta G_0 + RT \ln\left(\frac{P_M{}^m P_N{}^n}{P_A{}^a P_B{}^b}\right) \tag{2-10}$$

where ΔG_0 is the standard Gibbs free energy change for the reaction,

$$\Delta G_0 = m g_M{}^0 + n g_N{}^0 - a g_A{}^0 - b g_B{}^0 \tag{2-11}$$

g_i^0's are the standard Gibbs free energies of the constituents.

Equation 2-10 gives the Gibbs free energy change for the reaction. We are interested on how is that energy change is related to the work the system has performed. To find that relation, consider the following thermodynamic identity for a reversible process, ($dQ = TdS$)

$$dG = -\delta W + PdV + VdP - SdT \tag{2-14}$$

At constant temperature and pressure, the above equation can be written as,

$$dG = -\delta W + PdV \tag{2-15}$$

Since it is a non-expansion work, equation 2-15 takes the form,

$$dG = -\delta W_e \tag{2-16}$$

i.e. the change in Gibbs free energy of the reaction is equal to the maximum electrochemical work, W_e, that can be extracted when reactants *A* and *B* react to give products *M* and *N* under constant temperature and pressure conditions through a reversible reaction.

Now, we can focus on how the maximum electrochemical work relates to the EMF of the cell. The EMF produced due to half-cell reactions drives the electrons to move from the anode to the cathode. If n_e mole of electrons move from anode to cathode per unit time and the EMF of the cell is *E*, the power extracted is simply EMF multiplied by the current,

$$W_e = n_e F E \tag{2-17}$$

where F is the total charge of 1 mole of electrons, known as Faraday's constant. Now if we look at the integral form of equation 2-16 combined with 2-17, we get,

$$\Delta G = -n_e F E \tag{2-18}$$

Applying Equation 2-18 to Equation 2-10 we get what is known as Nernst equation,

$$E = E_0 - \frac{RT}{n_e F} \ln\left(\frac{P_M{}^m P_N{}^n}{P_A{}^a P_B{}^b}\right) \tag{2-19}$$

where E^0 is related to ΔG^0 by Equation 2-18.

For the reaction occurring in an SOFC,

$$H_2 + 1/2O_2 \rightarrow H_2O$$

the reversible potential can be written as,

$$E = E_0 - \frac{RT}{2F} \ln\left(\frac{P_{H2O}}{P_{H_2} P_{O_2}{}^{1/2}}\right) \tag{2-20}$$

This maximum theoretical voltage, E, is also known as "Open Circuit Voltage" OCV and can be measured when there is no current in the circuit. Also, it can be observed, that to get the maximum OCV, a high concentration of reactants is required [FCH, 2004].

Equation 2-20 gives the maximum OCV but this is not the operating voltage of the fuel cell. The operating voltage is always less than the OCV due to the losses associated with the current production. There are three major types of voltage losses or polarization: activation, ohmic and diffusion and each type dominates over a certain operating range of the fuel cell.

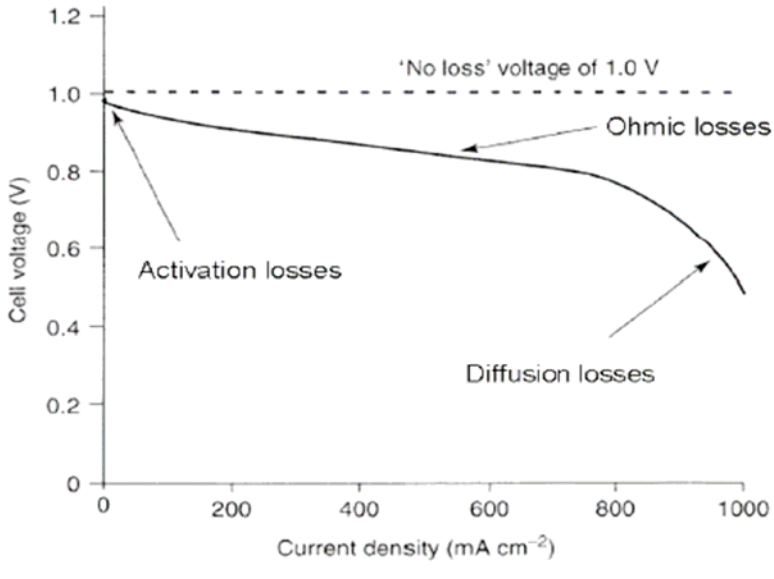

Figure 2-2 Current-Voltage Characteristics of a Fuel Cell Operating at 1073K [Larminie, 2000]

Activation Polarization is associated with the energy intensive activities of the making and breaking of chemical bonds at the electrodes. At the cathode, the incoming oxygen enters a reaction site and draws electrons from the catalyst to form oxygen ions. The resulting ions form bonds with the catalyst surface while electrons remain near the catalyst until another oxygen molecule begins to react with the catalyst, thus breaking the bond with the ion. The energy input to break the bond with the ion determines whether the electron will bond again with the catalyst, or will remain with the ion. A similar procedure occurs at the anode. The incoming hydrogen is broken up into its components by the catalyst where it draws oxygen ions to form water and electrons are released on the anode. The amount of energy needed for these activities of breaking and forming of chemical bonds comes from the fuel, and thus reduces the overall energy the cell can produce. If the reaction rate increases (i.e. high current density), the fuel flow rate must also increase which increases the kinetics and thus lowers the energy required to break bonds. Therefore when the current requirement is low, the overall cell polarization is dominated by the activation losses (Figure 2-2). Other factors, which lower the activation polarization, are increasing temperature, active area of the electrode, and activity of electrodes by the use of suitable catalyst [Angrist, 1965].

Ohmic polarization is caused by the electrical resistance the charge has to overcome when traveling across the different materials or interfaces. The resistances of the current collectors, electrodes, and the electrolyte are all factors which add to the energy loss. Resistance is added by the electrodes because of the contact resistance with the current collectors, with the electrolyte and through the electrode material itself. The electrolyte can add to the ohmic polarization through the resistance to ionic flow [FCH, 2004, and Angrist, 1965].

Concentration polarization is also termed diffusion polarization. It results from restrictions to the transport of gases to the reaction sites. This usually occurs at high current densities (Figure 2-2) because the rate at which hydrogen is consumed at reaction sites is higher that the rate of diffusion. The scarcity of hydrogen at the reaction sites effectively reduces the electrode activity leading to a corresponding loss in output voltage. This polarization is also affected by the physical restriction of the transfer of a large atom, oxygen, to the reaction sites on the cathode side of the fuel cell. Concentration polarization can be reduced by increasing the gas pressure and fuel concentration, using high surface area electrodes, or using thinner electrodes which shortens the path of the gas to the reaction sites [FCH, 2004], and [Angrist, 1965].

The combination of all the three polarizations affects the overall operating voltage. Each polarization dominates at a different current density range. Figure 2-2 shows that when there is no current in the circuit the OCV is reduced by the activation polarization. As the current increases, the activation polarization continues to decreases the operating voltage but the rate of reduction decreases in a parabolic manner. For moderate current densities, the ohmic polarization dominates and the polarization curve remains more or less a straight line. There is an inflection point observed at certain value of current density and afterwards the concentration polarization dominates. Mathematical expressions for each of these losses are described later.

As mentioned earlier, the efficiency of the fuel cell is not restricted by the Carnot limit. Because of the isothermal nature, most of the chemical energy released in the chemical reaction is converted to electrical energy instead of being consumed to raise the products temperature. Hence, the electrochemical processes offer high conversion efficiencies. The first law efficiency of a solid

oxide fuel cell based upon the lower heating value (LHV: since temperature is too high to let the water condense) is written as,

$$\eta_{th,cell} = \frac{n_e FE}{LHV} \tag{2-21}$$

2.1.2 MATERIALS

The importance of materials selection in solid oxide fuel cells comes from the fact that their operating temperature is very high. Besides being good conductors of ions and electrons, there are some other properties, which the materials should posses to ensure the stable and long term operation of the cell. Apart from the high strength of the materials, the thermal expansion of the electrodes, electrolytes and interconnects should be similar. The electrolyte and the interconnects must be dense enough to prevent gas mixing and the electrodes should be porous enough to allow the gas transport. Other important properties are related to the ease of manufacture and low cost. This section briefly discusses the materials used in a solid oxide fuel cell [FCH, 2004] ,[Larmine, 2000].

Electrolyte: Zirconia doped with 8-10 mole % of yttria (yttria-stablised zirconia) is generally used as electrolyte because of its high conductivity of oxygen ions and stability in both oxidizing and reducing environments. The conduction of oxygen ions is due to the fluorite structure of zirconia in which some Zr^{4+} ions are replaced by Y^{3+} ions leaving some O^{2-} sites vacant. These vacancies make O^{2-} ions from the cathode travel across the electrolyte. The ionic conductivity of YSZ compares to the liquid electrolyte and it can be made as thin as 25-50 μm to reduce ohmic losses. A small amount of alumina is also added to provide mechanical stability to the electrolyte.

Anode: The anode of a solid oxide fuel cell is a cermet (mix of a heat resistant compound and a metal) made by adding metallic nickel in the YSZ skeleton. The metallic nickel provides conductivity to the electrons and the YSZ provides stability and high porosity (20-40%) for the anode gases. The thermal expansion coefficient is close to that of the electrolyte.

Cathode: Similarly to the anode, the cathode of a solid oxide fuel cell should possess ionic and electronic conduction, high porosity, stability at high temperatures, and appropriate thermal expansion coefficient. Strontium doped lanthanum magnetite $(La_{0.84}Sr_{0.16})MnO_3$ a p-type semiconductor is most commonly used for cathode material.

Interconnect: The interconnect in a fuel cell is used to connect individual cell units in series. In a planar solid oxide fuel cell stack, it is also known as bipolar plate as one side of it is in contact with the cathode and the other side with the anode. Apart from conducting electrons from the anode to the cathode, it provides space for the flow channels for fuel and air. The arrangement is different in a tubular solid oxide fuel cell, which is discussed later in this chapter. Choosing the right material for the interconnect is a difficult task due to the operating temperature of the SOFC (800 to 1000^0C): conventional metals like steel differ in thermal expansion coefficient with the YSZ electrolyte. One material that suits, “inconel” type stainless steel, tends to be very expensive. Other metals tend to form an oxide coating, which limits their electrical conductivity and act as a barrier to the mass transport in the flow channels [Larminie, 2000]. Lanthanum chromite, which is

basically a ceramic, is commonly used for tubular designs. The conductivity of the material is enhanced by doping it with magnesium or other alkaline earth elements. Most of the fabrication methods of these alloys are proprietary and considerable research is going on in this field.

2.1.3 PRACTICAL DESIGSN AND STACKING

The three main SOFC arrangements are: tubular, planar and monolithic. These arrangements differ in their complexity, sealing methods, losses, and power density. The highest power density is achieved with the monolithic design, which looks like a corrugated card box in its cross section. However, difficulties with the sealing and thermally induced tensions, which cause the breaking of the cell, favor the tubular, planar or the combination of the two arrangements.

Tubular Design: Siemens Westinghouse Power Corporation first developed the tubular design of a solid oxide fuel cell. Figure 2-3 shows the schematic and stacking arrangement. The cell unit is in the form of a hollow cylindrical tube closed at one end. Air channel, cathode, electrolyte, anode, and fuel channel are arranged in layers from the center to the periphery. In this design, thin layers of electrolyte and anode are deposited on a cathode tube. The tube is produced by extrusion and sintering. A strip of interconnect is tightly attached to the cathode and the other end of it is in contact with the anode of the adjacent cell unit. Air is supplied in the inner tube and fuel to the free side of the anode.

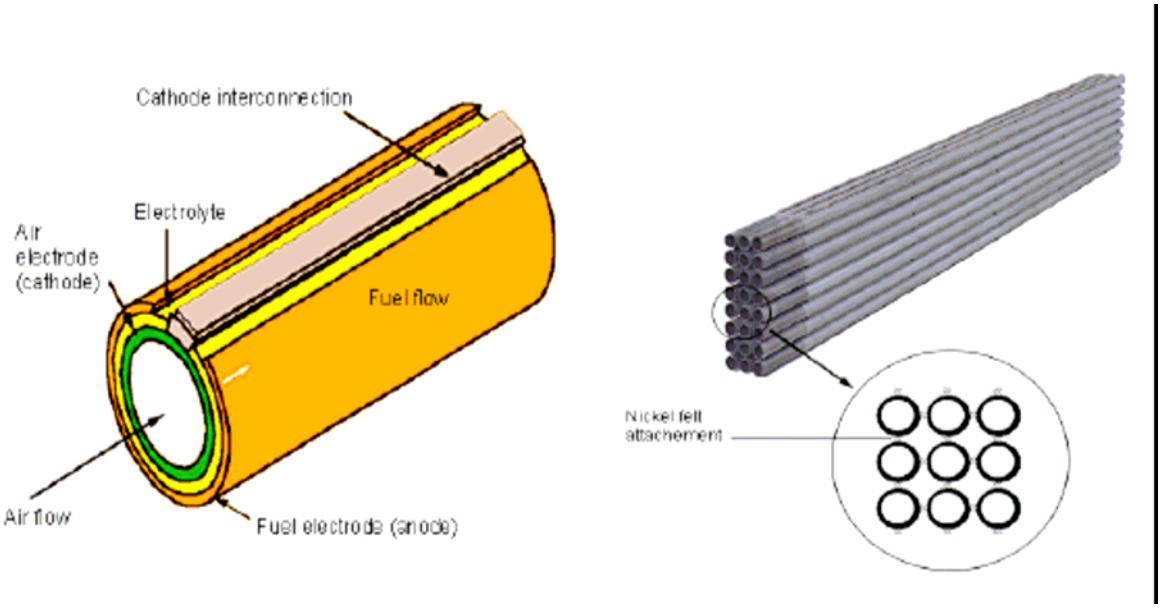

Figure 2-3 Tubular SOFC Developed by Siemens Westinghouse (left) and the Stacking of the Cells (right). (Siemens Westinghouse)

Figure 2-3 (right) shows a tubular fuel cell stack developed by Siemens Westinghouse, which consists of 24 tubes (each 2.2cm diameter and 150cm in length) connected in series[Larmine, 2000].

.

Planar Design: Planar solid oxide fuel cells are currently produced by a number of companies. Several geometries have been developed such as quadratic, circular or rectangular. Each unit

consists of flat plates of interconnect, cathode, electrode and anode and these units are put side by side to form cell stack (Figure 2-4).

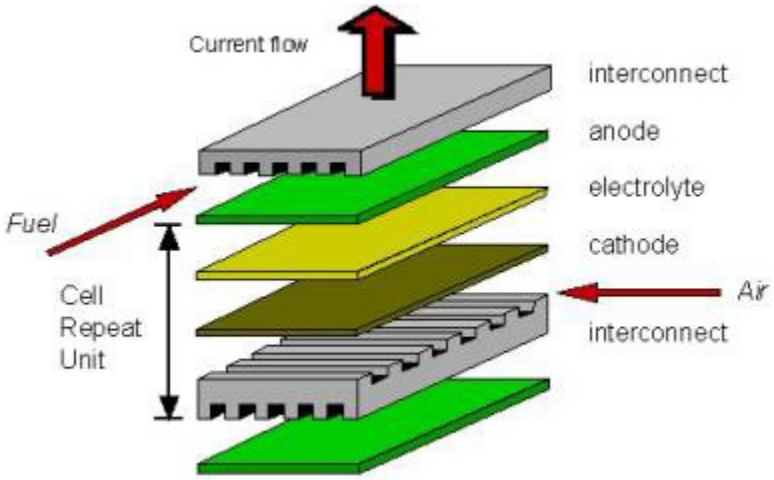

Figure 2-4 Flat Plate SOFC Unit (Craig Fisher)

Many flow arrangements exist in a planar SOFC, such as co-flow, counter flow and cross flow. The co-flow arrangement is the most favorable design in terms of thermal stresses where as the counter flow is the least favorable in terms of thermal gradient but is most commonly used due to the less complicated manifolding and the reduced constraints of sealants. Advantages of planar SOFC are ease of manufacture, simple design and high power density [Larmine, 2000].

Integrated planar SOFC and tubular SOFC design: Integrated planar SOFC design by Rolls Royce (Day, 2000) utilizes the features of both tubular and planar SOFC. It consists of an assembly of planar SOFCs fabricated in a ceramic housing which provides manifolding for the fuel gas and there are no separate bipolar plates instead interconnects are fabricated on to the cell housing itself [Larminie, 2000].

2.2 THE BOTTOMING CYCLE

As mentioned earlier that maximum work that can be extracted from a fuel cell is equal to the Gibbs free energy change of the reaction occurring in the cell. Figure 2-5 shows how fuel cell and heat engines efficiencies vary with temperature and how the combined cycle always gives a better performance.

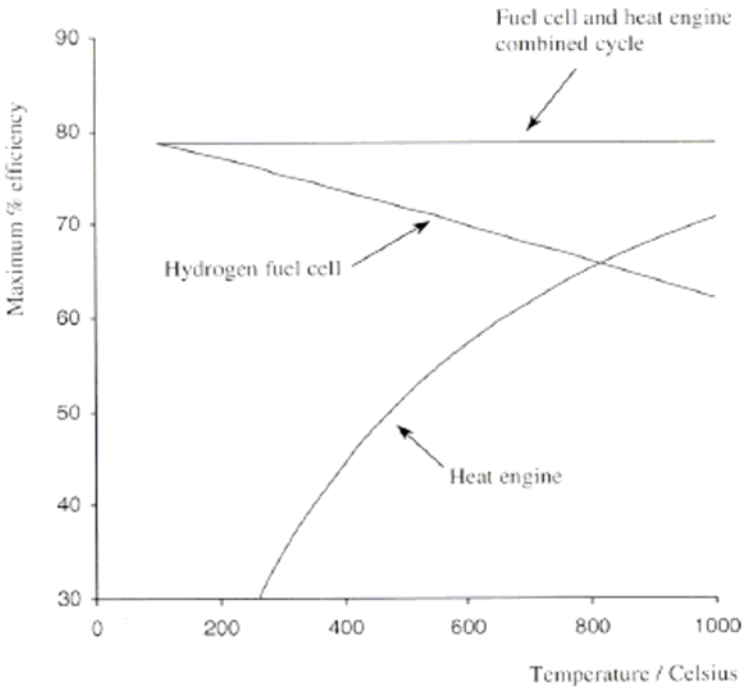

Figure 2-5 Comparison of Heat Engine, Hydrogen Fuel Cell and Combined Hybrid System Efficiency [Larminie, 2000]

From the above figure, we can fully appreciate the potential of hybrid systems. Traditional heat engines need to operate at really high temperatures to achieve considerable thermal efficiencies and the losses are higher in fuel cells at low temperatures. But at high operating temperatures, fuel cells combined with heat engines approach the maximum theoretical efficiency. This section discusses the various components and their role in the hybrid system.

2.2.1 GAS TURBINE

A gas turbine cycle is based on the Brayton cycle, which is a simple series of compression, combustion, and expansion processes. The main components of the cycle are a compressor, a combustor, and a gas turbine. The number of components is not limited to three as the cycle may consist of several compressors and turbines (expanders). Figure 2-6 illustrates the basic schematic of a gas turbine engine. The ambient air is compressed and sent to the combustor. The constant pressure combustion takes place and the exhaust is sent to the turbine where power is extracted to drive the compressor and the generator. Heat exchangers can also be used to preheat the stream entering the combustion chamber.

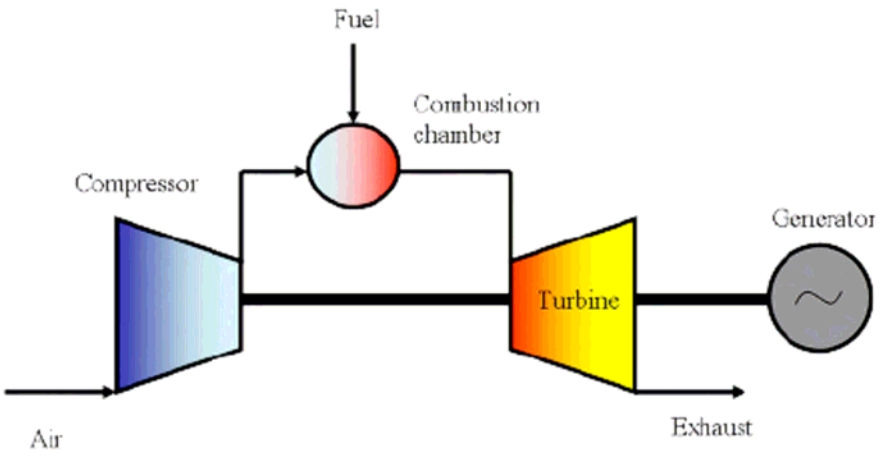

Figure 2-6 Schematic of a Gas Turbine Engine Based Upon the Brayton Cycle [Thorud, 2005]

Gas turbine engines are generally used for power production falling in the range of few kilowatts to several megawatts and offer an electrical efficiency of 30-40%. This can be further improved by adding a topping cycle to achieve efficiencies of up to 60%.

A gas turbine can be directly or indirectly connected to the SOFC. In an indirect integration, the combustor of the gas turbine is replaced with a heat exchanger in which air from the compressor is heated by the fuel cell exhaust and the SOFC can operate under atmospheric conditions. Although, it reduces the sealant requirement in the SOFC stack, the heat exchanger has to operate at very high temperatures and pressure differences. The material requirements in the indirect integration are really an issue and hence, it is not generally used.

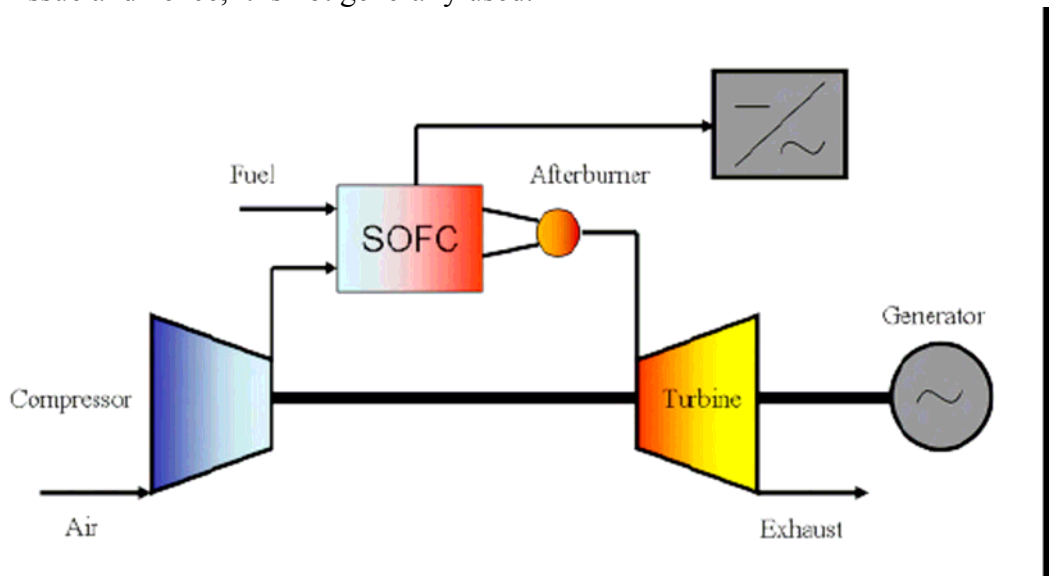

Figure 2-7 Gas Turbine Engine as a Bottoming Cycle in a SOFC-GT System [Thorud, 2005]

Figure 2-7 shows a direct integration of a solid oxide fuel cell and a gas turbine system. As can be seen from it, the combustion chamber of the gas turbine engine has been replaced with an SOFC and an afterburner. The pressurized stream from the compressor goes into the SOFC. The exhaust from the SOFC goes to the afterburner and the resulting high temperature and pressure exhaust

enters into the turbine. In this case, the SOFC operates at high pressure, which further improves its performance. Moreover, heat exchangers are added after the turbine exhaust to further utilize the waste heat in preheating of the streams entering the SOFC stack. The high-pressure operation of SOFC stack causes large pressure gradients between anode and cathode. This pressure imbalance needs to be avoided, due the brittleness of the SOFC materials, and good sealants are required to stop leakages [Larmine, 2000, and Thorud, 2005].

2.2.2 STEAM TURBINE

A standard Rankine cycle can also be used as a bottoming cycle in a SOFC hybrid system. Though SOFC and steam turbine systems are less complicated, they offer lower efficiency than SOFC/GT systems and are not suited for applications where weight of the overall system is an issue (e.g. aircraft applications, especially for short missions).

2.3 OTHER PLANT COMPONENTS

Depending upon the fuel used and the chosen configuration, stable operation of SOFC/GT systems may require components that have not been discussed so far. This section discusses the requirement and the role of these components in brief.

2.3.1 FUEL PROCESSING

One important feature of high temperature fuel cells is that they can work with other fuels like natural gas or any other hydrocarbons. Solid oxide fuel cells, operating on heating oil, fermentation [Jenne, 2002], methanol, formic acid [Saunders 2002], gasified coal and biomass, have also been reported. All of these fuels produce hydrogen through chemical reactions that occur at temperatures usually above 500 ^{0}C and are endothermic. The heat required by these reforming reactions is provided by the fuel cell.

Desulphurisation: It is necessary for some fuels like natural gas and petroleum to go through the desulphurization process before any further fuel processing is done. These fuels generally contain suphur in the form of organic compounds or H_2S, which acts as a deactivator for the steam reforming catalysts and shift reaction catalysts [Larminie, 2000]. Any organic sulphur-containing compounds are converted to H_2S in the presence of nickel-molybdenum oxide catalyst or cobalt-molybdenum oxide catalyst via "*hydrogenolysis reactions*" of the type:

$$(C_2H_5)_2S + 2H_2 \rightarrow 2C_2H_6 + H_2S \qquad (2\text{-}22)$$

the H_2S that is formed by such reactions is converted to zinc sulphide over a zinc oxide bed:

$$H_2S + ZnO \rightarrow ZnS + H_2O \qquad (2\text{-}23)$$

Steam reforming: Any fuel that is used in an SOFC has to be converted to hydrogen and carbon monoxide and the method that is generally practiced is the steam reforming. The basic reforming reactions from methane and other hydrocarbons C_mH_n are:

$$CH_4 + H_2O \rightarrow CO + 3H_2 \qquad [\Delta H = 206kJ/mole] \qquad (2\text{-}24)$$

$$C_nH_m + nH_2O \rightarrow nCO + (m/2 + n)H_2 \qquad (2\text{-}25)$$

$$CO + H_2O \rightarrow CO_2 + H_2 \qquad [\Delta H = -41kJ/mole] \qquad (2\text{-}26)$$

The reforming reactions 2-24 and 2-25 are termed as *oxygenolysis reactions* and reaction 2-26 as *water gas shift reaction* and generally occur in presence of nickel catalyst in a solid oxide fuel cell at temperature above 500 ^{0}C. These reforming reactions are reversible and reach equilibrium very fast over the active catalyst. The combination of reactions 2-24 and 2-26 makes sure that the overall product is a mixture of mainly CO, H_2, and CO_2 together with remaining methane and steam [Larminie, 2000].

There are two methods of steam reforming: "direct internal reforming (DIR)" and "indirect internal reforming (IIR)". When the reforming reactions take place directly over the anode of the SOFC, reforming is termed as DIR. DIR often better utilizes the steam and provides a higher degree of thermal integration but it increases the system complexity. In the case of indirect internal reforming (IIR), there is a separate reformer, which is either thermally integrated with the stack or to an external heat supply [Larminie, 2000].

2.3.2 COMBUSTOR/AFTERBURNER

The combustor in a SOFC/GT hybrid system is used after the fuel cell stack to burn the remaining fuel (generally the fuel utilization in a SOFC stack is around 80%). The combustor should be specifically designed for the hybrid system; a commercial combustor cannot be used because the exhaust from the SOFC has a very low calorific value and diluting air is not at once available at sufficient temperature. However, combustors specifically designed for an SOFC can operate over a large range and at the same time achieve very low emissions [Hermann, 2002].

2.3.3 HEAT EXCHANGERS

Heat exchangers in an SOFC system are of great importance since the gasses entering the SOFC need to be preheated for better performance and to reduce thermal stress in the stack. The heat exchangers also affect the overall efficiency and optimum operating pressure of the system.

2.3.4 OTHER COMPONENTS

There are other components such as supply pumps, power electronics, piping, etc. that come into the design of the actual power plant. The discussion of these components has been omitted in the presented document.

3. LITERATURE REVIEW

The aim of this chapter is to establish a platform for the modeling presented in the next chapter. After going through this chapter, the reader would be able to understand the current state of the art and where the presented work fits in.

Modeling of solid oxide fuel cells has been an area of research since 1980's and there have been a lot of models developed so far. Initial models were lumped mass models and there were a lot of uncertainties in the results due to lack of experimental data. Increasing experimental research during early 90's focused many such issues and established many empirical relationships to accurately predict the performance of the cell. Also, due to the increase in calculation capabilities, it was possible to create more detailed models. During the late 90's, several projects were initiated for detailed single cell modeling. Today modeling research is pursued in both detailed single cell modeling and system level stack modeling. Nevertheless, lumped models still continue to attract the attention of researchers due to their simplicity and small calculation time. Lumped models are considered over detailed models when it comes to predict the cells performance in an overall hybrid cycle. Many calibrated cell models have been created and overall thermodynamic or electrical performance can be predicted quite accurately even for lumped models of the fuel cell.

3.1 DIFFERENT MODELING APPROACHES

Depending upon the application, different models are available in the open literature and there are large differences in the level of details in the models presented. This chapter presents a review of the work of selected authors relevant to the model developed in the present work. A good summary of the development of SOFC models is presented by [Thorud, 2005]. Lumped models have been center of attention and have been largely used for studies of different cycle configurations [Winkler, 2000], [Rao, 2001] and to some extent for part-load studies [Campanari, 2000], [Costamagna, 2001], and [Chan, 2002]. As mentioned earlier, the great benefit of using lumped models is simplicity of the model development and short calculation time. A large amount of experimental data and mathematical relations exists for components such as compressors, turbines and heat exchangers, so these components can be modeled fairly accurately despite the lumped approach [Desideri, 2005]. The lumped approach in SOFC models also facilitates uncomplicated changes between different geometries, as this only involves changes in geometry specific parameters. Accordingly, lumped models are also easier to adjust to experimental data. The disadvantage of lumped SOFC models is that they can only account for mean values of the parameters and it follows that more detailed investigation of the cell is needed to check for undesirable effects such as thermal cracking, coking or exceeding temperature limits locally [Magistri, 2002]. This problem may be partly avoided by using a lumped model for system calculations, and a detailed model to test the validity of the results. Obviously, implementing a detailed SOFC model in the system model gives the most accurate results and this approach has been followed in [Palsson, 2000]. In this work a lumped SOFC model [PNNL, 2002] created in Microsoft excel by the Pacific Northwest National Laboratory has been used to optimize the cycle

configuration and further performance analysis. The model is based on theoretical fundamentals and has been calibrated empirically.

3.2 HYBRID SYSTEM CONFIGURATIONS

Many of configurations found in literatures use a basic recuperated gas turbine integrated with an SOFC. Figure 3-1 shows such a model when hydrogen is used as a fuel. In case of internal reforming (natural gas as fuel), an internal reformer is generally added between the fuel heat exchanger and the SOFC and is fed by the anode exhaust to provide steam for internal reforming. Most of the studies of this system focus on optimizing the steady state operational parameters such as operating pressure, cell voltage and turbine inlet temperature (TIT). This type of systems has been investigated in [Palsson, 2002], [Campanari, 2000], and [Costamagna, 2001]. The electrical efficiency predictions for the system are in the range of 58-65% for sub MW-class units.

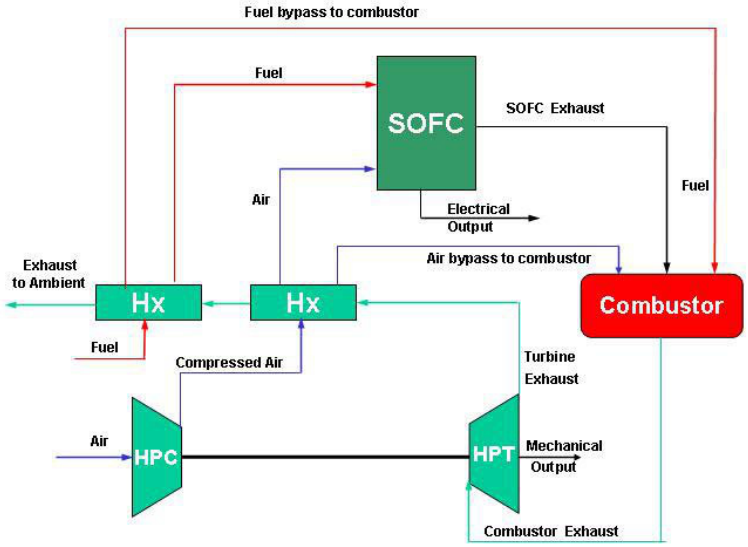

Figure 3-1 A Typical SOFC/GT Hybrid System

There are some improvements of the configuration as used in [Selimovic, 2002]. In the improved configuration, the SOFC stack has been replaced by two SOFC stacks connected in series with respect to gas flow. Due to the higher efficiency of the fuel cells compared to the gas turbine this would increase the total electric efficiency from 60.5% to 65.2%. A similar kind of configuration is used in [Winkler, 2000] with three SOFC stacks connected in series but the difference is that the streams pass through the expanders in order to cool the cathode air. The pressure ratio used in this process is around 15-20 and the system efficiency is predicted to be above 80%. Even higher pressure ratios are suggested in [Yi, 2004]. In this paper a pressure ratio of 50 for a process with an inter-cooled compressor and a two-stage expansion is suggested

3.2 MOTIVATION

The presented work is an attempt to model a hybrid system for aircraft applications and is inline with NASA Glenn research center (GRC) work [Freeh, 2005] and [Steffen, 2005]. Some of the tools used by GRC have been ASPEN and Numerical Propulsion System Simulation (NPSS). The aim of GRC is to develop an efficient tool in Matlab-Simulink, which could simulate a hybrid system with sufficient accuracy. The reasons to use Matlab, according to GRC, are that the Matlab package is relatively cheap and commonly used among academic institutions. The author's work can be seen as a developmental step to model a hybrid system, which satisfies the GRC needs and requirements. Figure 3-2 shows the system modeled in ASPEN by GRC.

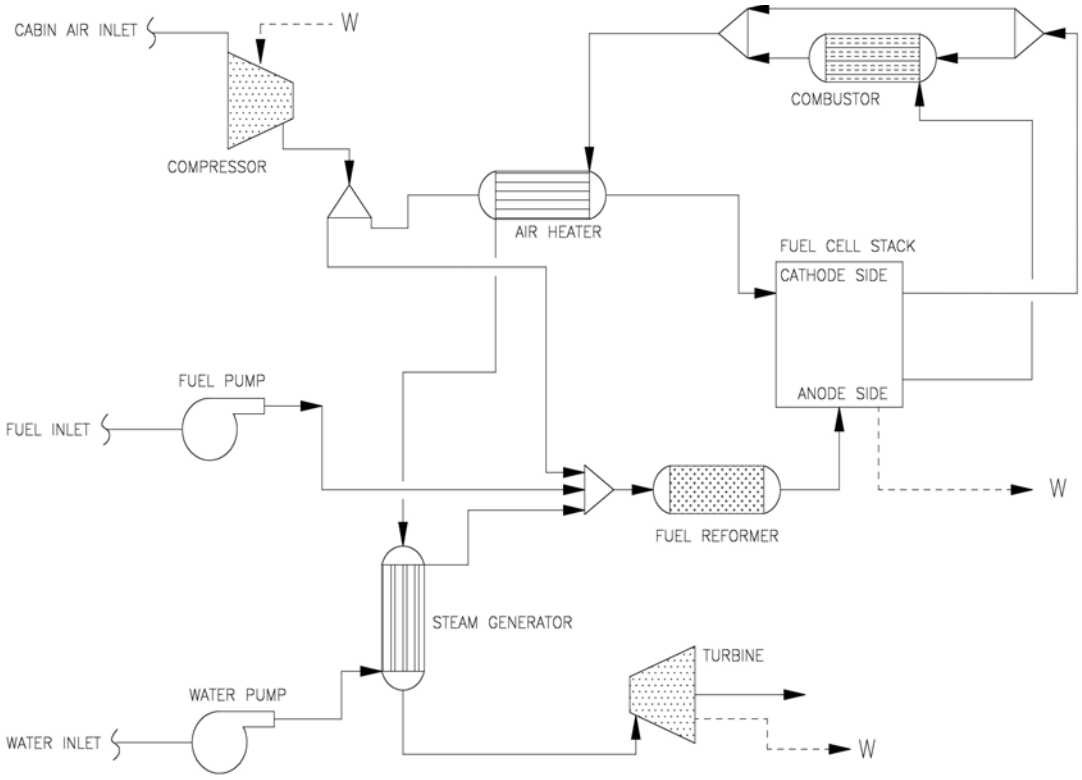

Figure 3-2 ASPEN Model of SOFC/GT Hybrid System by NASA Glenn Research Center [CAPS, 2005]

4. MODELING OF SOFC-GT SYSTEMS

This chapter presents the mathematical modeling of the SOFC-GT hybrid system. As discussed in chapter 3, SOFC-GT hybrid systems differ in their configuration and modeling. Figure 4-1 represents the modeling methodology followed in this work.

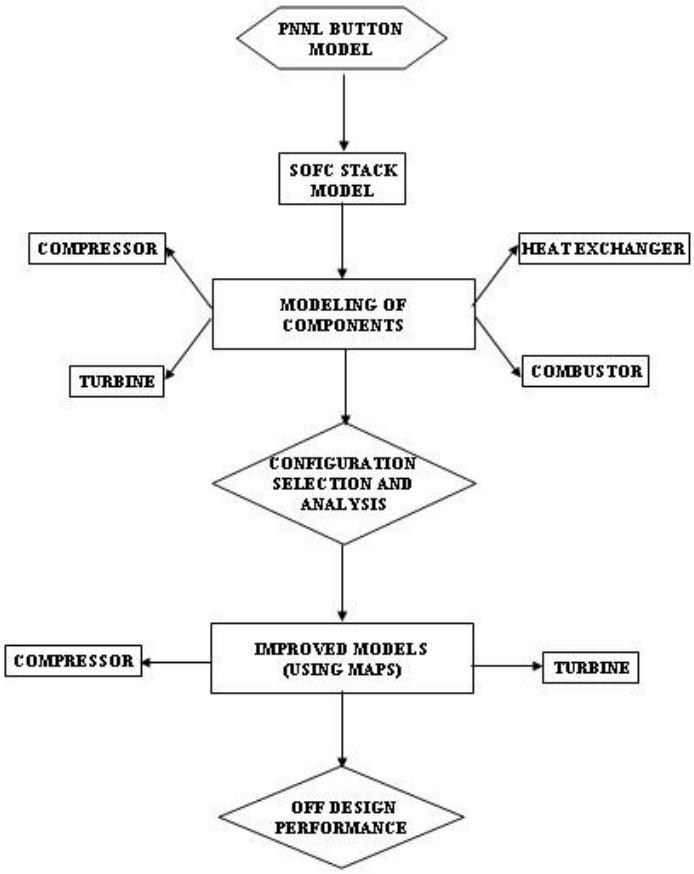

Figure 4-1 Flow Diagram for the Modeling Methodology Employed in this Work

The starting point of the modeling is the Pacific Northwest National Laboratory (PNNL) unit button cell model (details of which are explained later). A preliminary version of the model was implemented by our group in Matlab-Simulink and extended to create the transient SOFC stack model [Brinson, 2004]. A more recent version of the PNNL model [PNNL, 2002] has been implemented by the author in the Matlab-Simulink environment and adapted for hybrid system modeling. Models for the turbine, compressor, combustor, and heat exchangers have been developed. Based upon performance parameters such as the SOFC power, cycle efficiency, exhaust temperature, and turbine inlet temperature, different hybrid system configurations have been compared. Up to the configuration selection, the models for the turbine and compressor are based on simple thermodynamic relations that circumvent the complexity of comprehensive

models. Once the optimum configuration is selected, performance maps are used for design and off-design calculations.

4.1 SOLID OXIDE FUEL CELL MODELING

Based upon the PNNL's unit button cell model, a thermodynamically transient SOFC stack model has been developed in a Matlab-Simulink environment.

4.1.1 PNNL'S UNIT BUTTON CELL MODEL [PNNL, 2002]

The Pacific Northwest National Laboratory (PNNL) has developed a single SOFC button cell. The mathematical model of the button cell was implemented in a Microsoft Excel sheet to evaluate the voltage response for given current densities, fuel and air compositions, and cell temperature [PNNL, 2002] . The model performs a "unit-cell" calculation at steady state, assuming that fuel composition, air composition, and temperature are homogeneous over the active area. Although the form of the algorithm is based on theoretical treatments of the overpotential terms, several adjustable parameters are used to calibrate the model to closely match actual small-scale single-cell data that was taken over a range of temperatures and fuel compositions. The unit button cell model assumes a constant operating temperature, which is fixed experimentally using a furnace. The model assumes a two Kelvin degrees increase between the inlet and outlet streams. This assumption is not valid for stack calculations since the stack does not operate in a controlled environment. The details of this model are presented in the appendix.

4.1.2 STACK MODEL

4.1.2.1 HEAT LOSSES

The main difference with the button cell model is that the stack temperature is an unknown. The first law of thermodynamics can be used to compute the stack temperature. Here, it is assumed that the stack is insulated and therefore energy leaves through electrical work and the flow streams only. If we consider the polarization curve of the SOFC as shown in Figure 4-2, the cell always operates at a lesser voltage than the open circuit voltage at non-zero current. ${E^0}_H$ is called the thermal cell voltage and includes the $T\Delta S$ term and E^* is the operating voltage. The difference between the thermal voltage and operating voltage is related to the heat loss and is expressed by the equation 4-1,

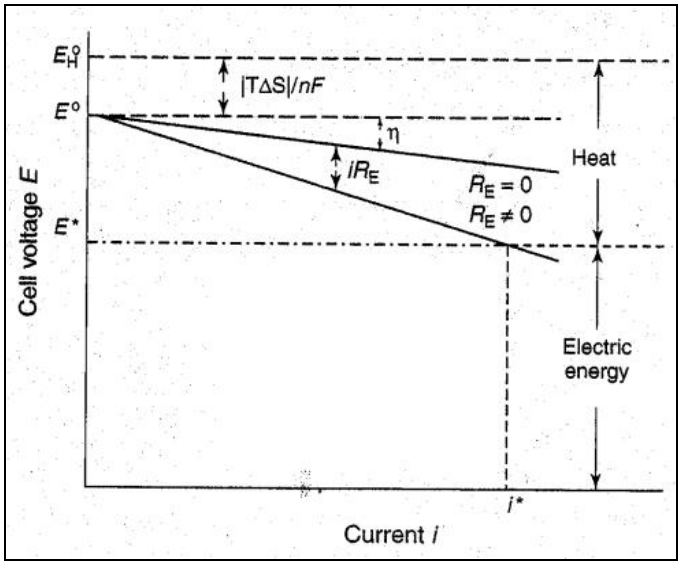

Figure 4-2 Typical I-V Polarization Curve of an SOFC

$$\dot{Q}_{Stack} = i \cdot \left(E_H{}^0 - E^* \right) \tag{4-1}$$

4.1.2.2 SIZING OF STACK

As mentioned earlier, the single cell model is extended into a stack model before creating a SOFC hybrid system. An operating point (Figure 4-3) is chosen and the corresponding current density and voltage are used to size the stack. Based on the given specifications (bus voltage), the number of cells required can be calculated.

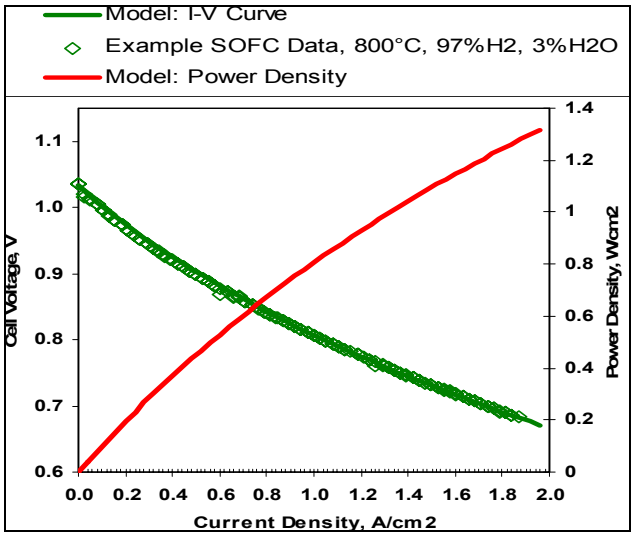

Figure 4-3 PNNL Single Cell Polarization Curve [PNNL, 2002]

In this work, a current density of 1 A/cm^2 was chosen. The corresponding single cell potential is .807 V (as indicated in Figure 4-3). The number of single cells required to form the stack is computed as

$$n_{cells} = \frac{V_{bus}}{V_{cell}} \tag{4-2}$$

Equation 4-2 assumes that the cells are arranged in series. Similarly, the area of each cell within the stack can be calculated using the single cell current density and the stack current:

$$A = \frac{\left(\frac{\dot{W}_{\max}}{V_{bus}} \right)}{i_{cell}} \tag{4-3}$$

4.1.2.3 TRANSIENT ANALYSIS

By applying the first law of thermodynamics to the fuel cell, it is possible to account for temperature transients due to system changes.

$$\frac{dE_{Stack}}{dt} = \dot{Q}_{Stack} - \dot{W}_{Stack} + h_{in} - h_{out} \tag{4-4}$$

or,
$$(MC)_{Stack} \frac{dE_{Stack}}{dt} = \dot{Q}_{Stack} - \dot{W}_{Stack} + H_{in} - H_{out} \tag{4-5}$$

Where,

$\dot{Q}_{Stack}$ – heat generated within the stack
$\dot{W}_{Stack}$ – net electrical work
H_{in} – enthalpy coming into the control volume (i.e. reactants)
H_{out} – enthalpy leaving the control volume (i.e. products)

The following table includes parameters required to estimate $(MC)_{Stack}$ once the the active cell area is known (Equation 4-3),

Table 4-1 Cell Material Properties and Components Thickness

	Specific heat capacity (J/kg*K)	Mass density (kg/m3)	Thickness (m)
Anode	466	4200	6 x 10-4
Cathode	520	6350	5 x 10-5

TABLE 4-1 continued

	Specific heat capacity (J/kg*K)	Mass density (kg/m3)	Thickness (m)
Electrolyte	460	6010	1 x 10-5
Interconnect	800	7700	5 x 10-4

Equation (4-5) is a 1st order ODE and gives the transient response of the SOFC stack temperature.

4.2 COMPRESSOR MODEL

In a hybrid system, ambient air is compressed and supplied to the SOFC. In the current analysis, the model of the compressor is based on perfect gas equations and polytropic transformations. The inputs to the model are the air flow rate and the required pressure ratio. The outputs are the overall efficiency, the exit stream temperature, and the power required to drive the compressor.

The process is assumed to be polytropic with polytropic efficiency, $\eta_{\infty c}$ (small stage efficiency):

$$\eta_{\infty c} = \frac{dT_s}{dT} \tag{4-6}$$

Where '*dT'* is the change in temperature in going from pressure '*P'* to '*P* + *dP'* and dT_s is the isentropic change in temperature corresponding the same pressure change.

For isentropic process,

$$T_s = C \times p^{\frac{\gamma_a - 1}{\gamma_a}}, \tag{4-7}$$

where 'C' is a constant and γ_a is the specific heat ratio. Differentiating equation 4-7 we get,

$$dT_s = C \frac{\gamma_a - 1}{\gamma_a} \frac{p^{\frac{\gamma_a - 1}{\gamma_a}}}{P} dp \tag{4-8}$$

and,

$$dT_s = \frac{\gamma_a - 1}{\gamma_a} \frac{T}{P} dp \tag{4-9}$$

Let's consider that pressure changes from P_i to P_e and the temperature changes from T_i to T_e. Equations 4-6 and 4-9 give,

$$dT = \frac{\gamma_a - 1}{\gamma_a \eta_{\infty C}} \frac{T}{P} dp \tag{4-10}$$

$$T_e = T_i \left(\frac{p_e}{p_i} \right)^{\frac{\gamma_a - 1}{\gamma_a \eta_{\infty C}}} \tag{4-11}$$

Once the exit temperature of the air stream is known, the enthalpy change is calculated using the following relation:

$$\Delta h_c = h_e - h_i = C_{p\,a}(T_e - T_i),$$

$$\Delta h_c = C_{p\,a} T_i (T_e / T_i - 1) \tag{4-12}$$

Using Equation 4-11, it can be rewritten as

$$\Delta h_c = C_{p\,a} T_i \left(\left(\frac{p_e}{p_i} \right)^{\frac{\gamma_a - 1}{\gamma_a \eta_{\infty C}}} - 1 \right) \tag{4-13}$$

If the isentropic temperature at the exit is T_{se}, the overall efficiency (isentropic) of the compressor is calculated by:

$$\eta_c = \frac{T_{se} - T_i}{T_e - T_i} \tag{4-14}$$

$$\eta_c = \frac{T_{se} / T_i - 1}{T_e / T_i - 1} \tag{4-15}$$

For an isentropic process,

$$\frac{T_{se}}{T_i} = \left(\frac{P_e}{P_i} \right)^{\frac{\gamma_a - 1}{\gamma_a}} \tag{4-16}$$

Combining Equations 4-15 and 4-16 gives,

$$\eta_c = \frac{\left(\frac{p_e}{p_i} \right)^{\frac{\gamma_a - 1}{\gamma_a}} - 1}{\left(\frac{p_e}{p_i} \right)^{\frac{\gamma_a - 1}{\gamma_a \eta_{\infty c}}} - 1} \tag{4-17}$$

Knowing the mass flow rate of air through the compressor, $\dot{m}_{air}$, the mechanical power consumed is given by,

$$\dot{W}_C = \dot{m}_{air} \Delta h_c \tag{4-18}$$

4.3 TURBINE MODEL

The turbine is used to drive the compressor and as a secondary electrical power device. The turbine has been modeled in a similar way as the compressor. With a given expansion ratio, turbine inlet temperature, and polytropic efficiency, the model outputs the exhaust temperature, the power

output, and the overall efficiency of the turbine. The following equations model the gas turbine for a uniform polytropic expansion,

The exhaust temperature:

$$T_e = T_i \left(\frac{p_e}{p_i} \right)^{\frac{(\gamma_g - 1)\eta_{\infty T}}{\gamma_g}} \tag{4-19}$$

The above equation is derived in the same way as equation (4-11) with a turbine polytropic efficiency of $\eta_{\infty T}$ defined as:

$$\eta_{\infty T} = \frac{dT}{dT_s} \tag{4-20}$$

The change in enthalpy:

$$\Delta h_T = C_{pg} T_i \left(\left(\frac{p_e}{p_i} \right)^{\frac{(\gamma_g - 1)\eta_{\infty T}}{\gamma_g}} - 1 \right) \tag{4-21}$$

The gas turbine efficiency,

$$\eta_T = \frac{1 - \left(\frac{p_e}{p_i} \right)^{\frac{(\gamma_g - 1)\eta_{\infty T}}{\gamma_g}}}{1 - \left(\frac{p_e}{p_i} \right)^{\frac{\gamma_g - 1}{\gamma_g}}} \tag{4-22}$$

Now, the mechanical power delivered by the gas turbine can be calculated as:

$$\dot{W}_T = \dot{m}_g \Delta h_T \tag{4-23}$$

where $\dot{m}_g$ is the gas flow rate through the turbine. Finally, the mechanical power delivered to the generator to produce electricity is,

$$\dot{W}_{net} = \dot{W}_T - \dot{W}_C \tag{4-24}$$

4.4 HEAT EXCHANGER MODELS

In a hybrid system, the heat exchangers are used to preheat the fuel and air streams from the hot exhausts. Two heat exchanger configurations have been used in the present analysis, parallel flow and counter flow. The following section explains the modeling concepts of both configurations.

4.4.1 PARALLEL FLOW CONFIGURATION

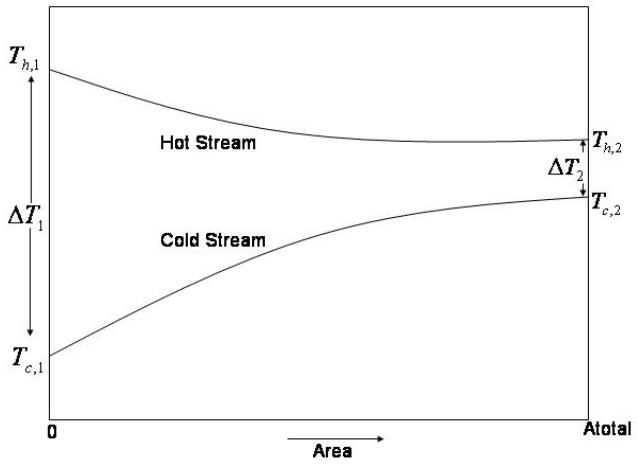

Figure 4-4 Parallel Flow Heat Exchanger Arrangement

A parallel flow heat exchanger model has been used in configurations 1 and 2A (the first two configurations explained later). Figure 4-4 shows the temperature profiles of hot and cold streams in a parallel flow heat exchanger. The model presented here calculates the exit streams temperatures for a given inlet conditions and heat capacities using the LMTD methodology,

$$\ln\left(\frac{\Delta T_1}{\Delta T_2}\right) = -\left(\frac{1}{C_h} + \frac{1}{C_c}\right) \tag{4-25}$$

where,
C_h- heat capacity of the hot stream
C_c- heat capacity of the cold stream
U- overall heat transfer coefficient
A- total heat transfer area

and, ΔT_1 and ΔT_2 are the stream-to-stream temperature differences in the front and back sections of the heat exchanger given by,

$$\Delta T_1 = T_{h,1} - T_{c,1} \tag{4-26}$$
$$\Delta T_2 = T_{h,2} - T_{c,2} \tag{4-27}$$

The proportionality between the total heat transfer rate, q, and the overall thermal conductance of the heat exchanger surface is,

$$q = UA\Delta T_{lm} \tag{4-28}$$

where, ΔT_{lm}, is the log mean temperature difference (LMTD) defined as,

$$\Delta T_{lm} = \frac{\Delta T_2 - \Delta T_1}{ln\left(\frac{\Delta T_2}{\Delta T_1}\right)} \tag{4-29}$$

Once *'q'* is known, the exit streams temperatures are calculated in the following way,

$$q = \int_{T_{h,1}}^{T_{h,2}} CdT = \int_{T_{c,1}}^{T_{c,2}} CdT \tag{4-30}$$

4.4.2 COUNTER FLOW CONFIGURATION

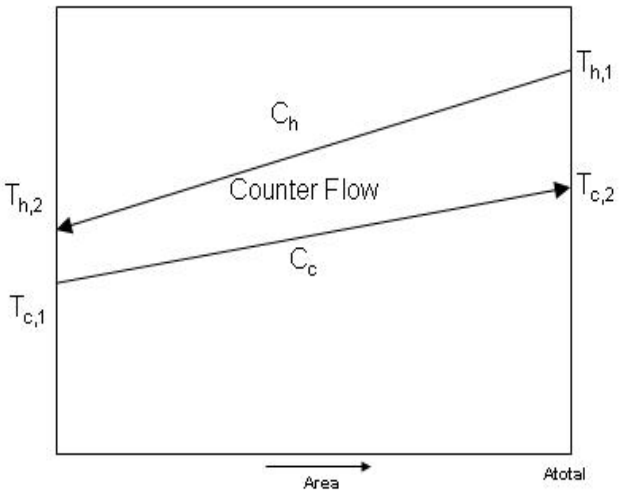

Figure 4-5 Counter Flow Heat Exchanger Arrangement

A counter flow configuration, Figure 4-5, is used for configurations after 2A. The model is based on the Effectiveness-NTU methodology, which makes use of two non-dimensional groups: the number of heat transfer units, NTU, and the effectiveness, ε, defined below.

Number of heat transfer units,

$$NTU = UA / C_{min} \tag{4-31}$$

where, $C_{\min}$, is the smaller of two heat capacities of hot and cold streams.

The heat exchanger effectiveness is defined as the ratio of actual heat transfer rate, *q*, and the maximum possible heat transfer rate between the two streams, $q_{\max}$,

$$\varepsilon = q / q_{max} \tag{4-32}$$

where,

$$q_{max} = C_{min}(T_{h,1} - T_{c,1}) \tag{4-33}$$

$(T_{h,1} - T_{c,1})$ is simply the temperature difference between the two inlet ports, i.e. the largest temperature difference between two streams and hence defines the ceiling value for the heat transfer rates between the two streams.

$$\varepsilon = \frac{C_h(T_{h,1} - T_{h,2})}{C_{\min}(T_{h,1} - T_{c,1})} = \frac{C_h(T_{c,2} - T_{c,1})}{C_{\min}(T_{h,1} - T_{c,1})} \tag{4-34}$$

And from the effectiveness-NTU relation,

$$\varepsilon = \frac{1 - \exp\left[-NTU\left(1 - C_{\min}/C_{\max}\right)\right]}{1 - (C_{\min}/C_{\max})\exp\left[-NTU\left(1 - C_{\min}/C_{\max}\right)\right]} \tag{4-35}$$

Once effectiveness is calculated, the actual heat transfer rate can be obtained using Equation 4-32 and the exit temperatures of the hot and cold streams are given by,

$$\begin{aligned} T_{h,2} &= T_{h,1} - q/C_h \\ T_{c,2} &= T_{c,1} - q/C_c \end{aligned} \tag{4-36}$$

4.5 COMBUSTOR MODEL

The streams coming out of the fuel cell are mixed with additional fuel and air. The mixture is combusted to produce a high temperature exhaust, which is sent to the turbine. In the current modeling, the combustion is assumed to be at constant pressure. It is also assumed that all the energy released goes into the products, which leave the combustor at adiabatic flame temperature.

The first law of thermodynamics requires,

$$H(SOFC)_{exhaust} + H(Fuel)_{additional} + H(Air) = H_{mix} \tag{4-37}$$

The product temperature is computed from,

$$h_{mix} = \sum \int_{T_{ref}}^{T_f} Cp(T)dT \tag{4-38}$$

where, h_{mix}, is the net specific enthalpy of the mixture and the summation is done for all the species after the combustion. T_f is the adiabatic flame temperature. $Cp(T)$ is defined as a 3rd degree polynomial,

$$Cp(T) = a + b\left(T - T_{ref}\right) + c\left(T - T_{ref}\right)^2 + d\left(T - T_{ref}\right)^3 \qquad (4\text{-}39)$$

a, b, c, and d are constants specific to the gas. An important point to note here is that model assumes the complete combustion in the presence of excess air and there are no nitrogen oxides $\left(NO_x\right)$ formed during the combustion.

4.6 IMPROVED TURBINE & COMPRESSOR MODELS

The models for the turbine and compressor, discussed in the previous section are based on a simple thermodynamic approach. They cannot predict the off-design performance of the hybrid system. The compressor and turbine parameters change when they operate under off-design conditions and hence in order to predict their performance accurately, an approach based on performance maps has been adopted. The gas turbine model is divided into 4 sub-models, i.e. compressor map, compressor, turbine map and, turbine.

4.6.1 COMPRESSOR MAP MODEL

A compressor is generally designed for a basic set of delivery pressure, temperature, isentropic efficiency, and mass flow rate. These parameters depend upon the shaft speed, inlet temperature, pressure, and thermodynamic properties of the gas. When the compressor operates under this condition, it is often referred as design point operation. Operation under any other condition is referred to as off-design operation. Experimental results from off-design operation are often summarized in performance maps, in which the number of free variables is reduced by use of non-dimensional parameters for better readability. Dimensional analysis shows that constant corrected speed lines (N_{corr}, Equation 4–40) can be plotted in two charts with corrected flow rate ($\dot{m}_{corr}$, Equation 4–42) on the x-axis, and with isentropic efficiency (η) or pressure ratio (π, Equation 4–41) on the y-axis. In Equations 4–40 to 4–42 the subscripts 01 and 02 relate to the stagnation values at the entry and exit, respectively. T_a and P_a are the reference temperature and pressure . The performance map for the modeled radial compressor, based on [Kurzke, 2004], is shown in Figure 4-6.

$$N_{corr} = \frac{N}{\sqrt{T_{01}/T_a}} \qquad (4\text{-}40)$$

$$\Pi = \frac{P_{02}}{P_{01}} \qquad (4\text{-}41)$$

$$\dot{m}_{corr} = \frac{\dot{m}\sqrt{T_{01}/T_a}}{P_{01}/P_a} \qquad (4\text{-}42)$$

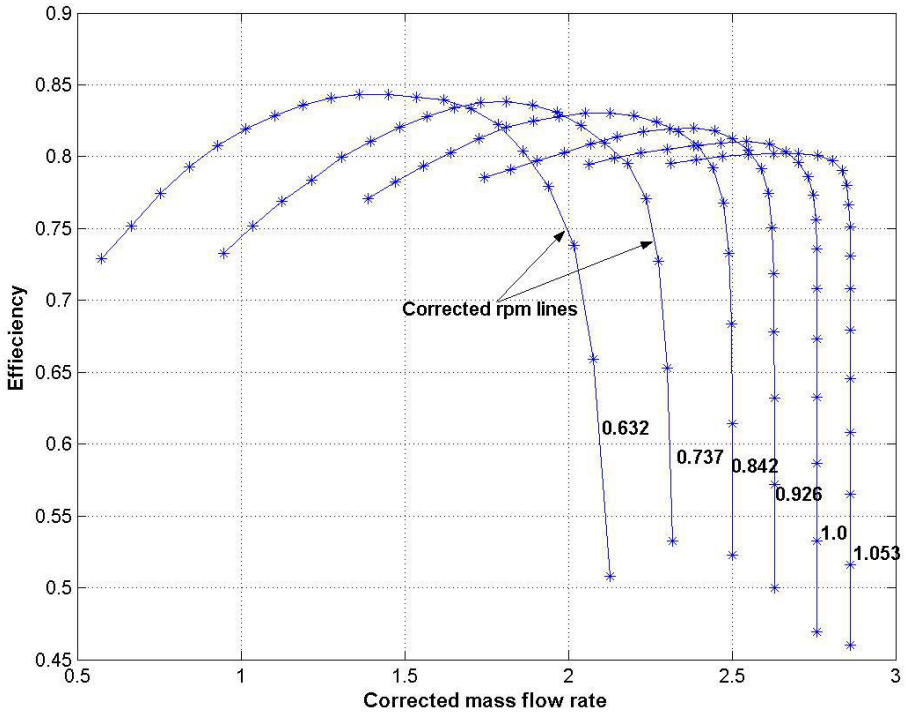

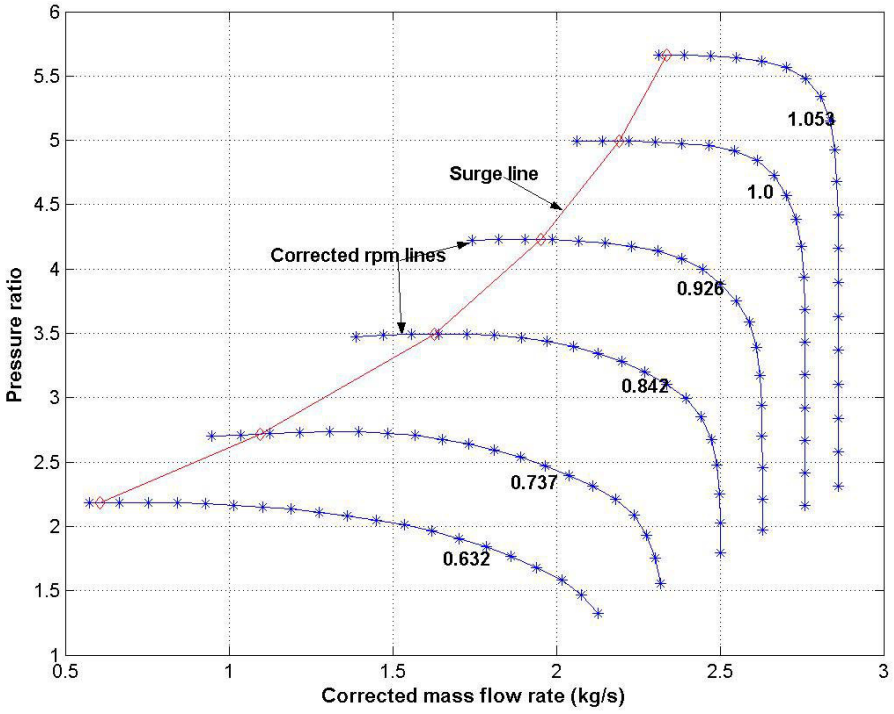

Figure 4-6 Performance Maps of the Modeled Compressor, Based on the DLR Radial Compressor Map

The red line in the bottom map of Figure 4-6, connects all the constant rpm lines and is called the surge line. Operation above this line may cause the compressor to surge and performance breakdown. Surge in a compressor occurs when there is insufficient mass flow or there is an aerodynamic stall in the initial stages of the compressor. In such cases, there is a complete break down of the flow field in the entire system and rapid changes in the mass flow lead to alternating stall and unstall behavior resulting in violent oscillations in pressure, propagation of press0075re waves, and failure of the entire compression system.

The benefit of the performance maps is that out of four parameters, if two parameters are known, the operating point can be located and the remaining parameters can easily be found. The maps shown in Figure 4-6 are specific maps and need to be non-dimensionalized before they can be used as generic maps. Equations 4-43 to 4-45 explain how the maps are non-dimensionalized to produce the generic maps.

$$N_{non\_dim} = \frac{N}{N_{DP}} \tag{4-43}$$

$$\Pi_{non\_dim} = \frac{\Pi}{\Pi_{DP}} \tag{4-44}$$

$$\dot{m}_{DP} = \frac{\dot{m}}{\dot{m}_{DP}} \tag{4-45}$$

where subscript '*DP*' in the above equations represents the design point values. In this study, experimental data for a radial compressor tested by DLR (Deutschen Zentrum für Luft und Raumfahrt) are used to obtain the corrected values in Equations 4–43 to 4–45. The data from this compressor can be found in the "Map Collection 2" assembled by Kurzke [Kurzke, 2004]. The same data has also been used in other SOFC/GT system studies [Chan, 2003]. The normalized off-design performance maps used in this model are depicted in Figure 4-7. The design point is the point where rpm, pressure ratio, and mass flow rate have the value 1. It should be noted that this off-design map is only valid for normalized shaft speeds in the range of 0.636 to 1.053 and below the surge line.

In most compressor applications, the risk of surge is avoided by operating a certain distance from the surge line. The distance to surge is often denoted as "surge margin". In this work the surge margin is defined according to equation 4–46.

$$\text{Surge Margin} = \frac{\Pi}{\Pi_{Surge}} \tag{4-46}$$

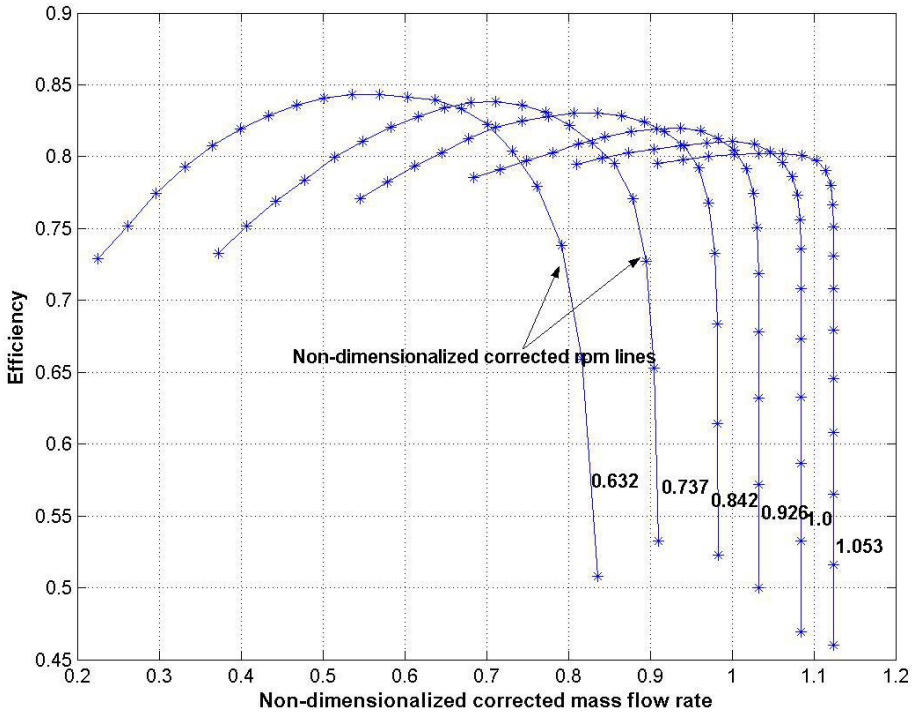

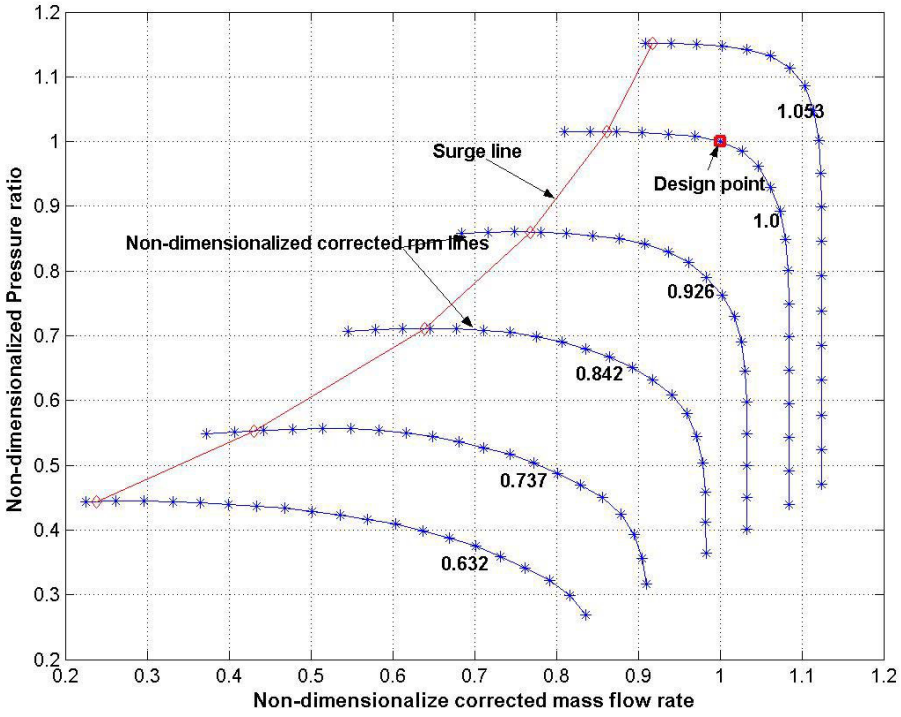

Figure 4-7 Normalized Performance Maps for DLR Radial Compressor

4.6.2 COMPRESSOR MODEL

The compressor model calculates the outlet temperature and the shaft speed for given inlet temperature, pressure, required pressure ratio, mass flow rate, and gas properties. These variables are further used to calculate the total power required to drive the compressor. The compressor operates under the following assumptions:

- Compressor is adiabatic.
- Gas kinetic energy is negligible i.e. stagnation and static conditions are the same
- There are no other losses except the ones described by the efficiency.

With the known design and operating conditions (required mass flow rate, pressure ratio, and inlet conditions) the operating point can be located on Figure 4-11. It is important to note that these maps have been implemented in a Matlab program and interfaced with Simulink to read the values during the program run. Once the operating point is located, the program calculates the shaft speed and the isentropic efficiency. The isentropic enthalpy change corresponding to the pressure change across the compressor, is calculated as,

$$\Delta h_{is} = Cp\left(T_{is} - T_i\right) \tag{4-47}$$

$$\Delta h_{is} = CpT_i\left(\frac{T_{is}}{T_i} - 1\right) \tag{4-48}$$

now, for an isentropic process,

$$\frac{T_{is}}{T_i} = \left(\frac{P_e}{P_i}\right)^{\frac{\gamma-1}{\gamma}} \tag{4-49}$$

hence, from the isentropic efficiency definition,

$$\Delta h = \frac{\Delta h_{is}}{\eta_C} \tag{4-50}$$

and the compressor power is,

$$\dot{W}_C = \dot{m}_{air}\Delta h \tag{4-51}$$

where, $\dot{m}_{air}$ is the air flow rate across the compressor. The exhaust temperature is calculated using the actual enthalpy change as:

$$T_e = T_i + \frac{\Delta h}{Cp} \tag{4-52}$$

4.6.3 TURBINE MAP MODEL

A turbine is generally choked while operating near the design point. The exit stream properties can be calculated from the choked flow condition using equation 4-53.

$$\frac{\dot{m}}{\dot{m}_{DP}} = \frac{P_i}{P_e}\sqrt{\frac{1-\left(\frac{P_e}{P_i}\right)^2}{1-\left(\frac{P_e}{P_i}\right)^2_{DP}}} \qquad (4\text{-}53)$$

Where the subscript *'DP'*, *'i', 'e'* represent the design point, inlet and outlet of the turbine, respectively. Figure 4-8 shows the generic performance map of the radial turbine used in the present modeling. The experimental data for the radial turbine is taken from the Kurzke's "Map Collection 2" referred to as NASA-CR-174646 [Kurzke, 2004]. As it can be seen from the generic maps, the turbine has a very large operation range in the choked condition. However, if the pressure ratio is low, the chocked assumption is no longer valid, and performance maps are required.

The maps shown in Figure 4-8 are specific to the NASA-CR-174646 turbine, and need to be normalized before they can be used for a generic turbine. The turbine maps have been normalized in the same way as the compressor using Equations 4-43 to 4-45. Figure 4-9 shows the normalized maps.

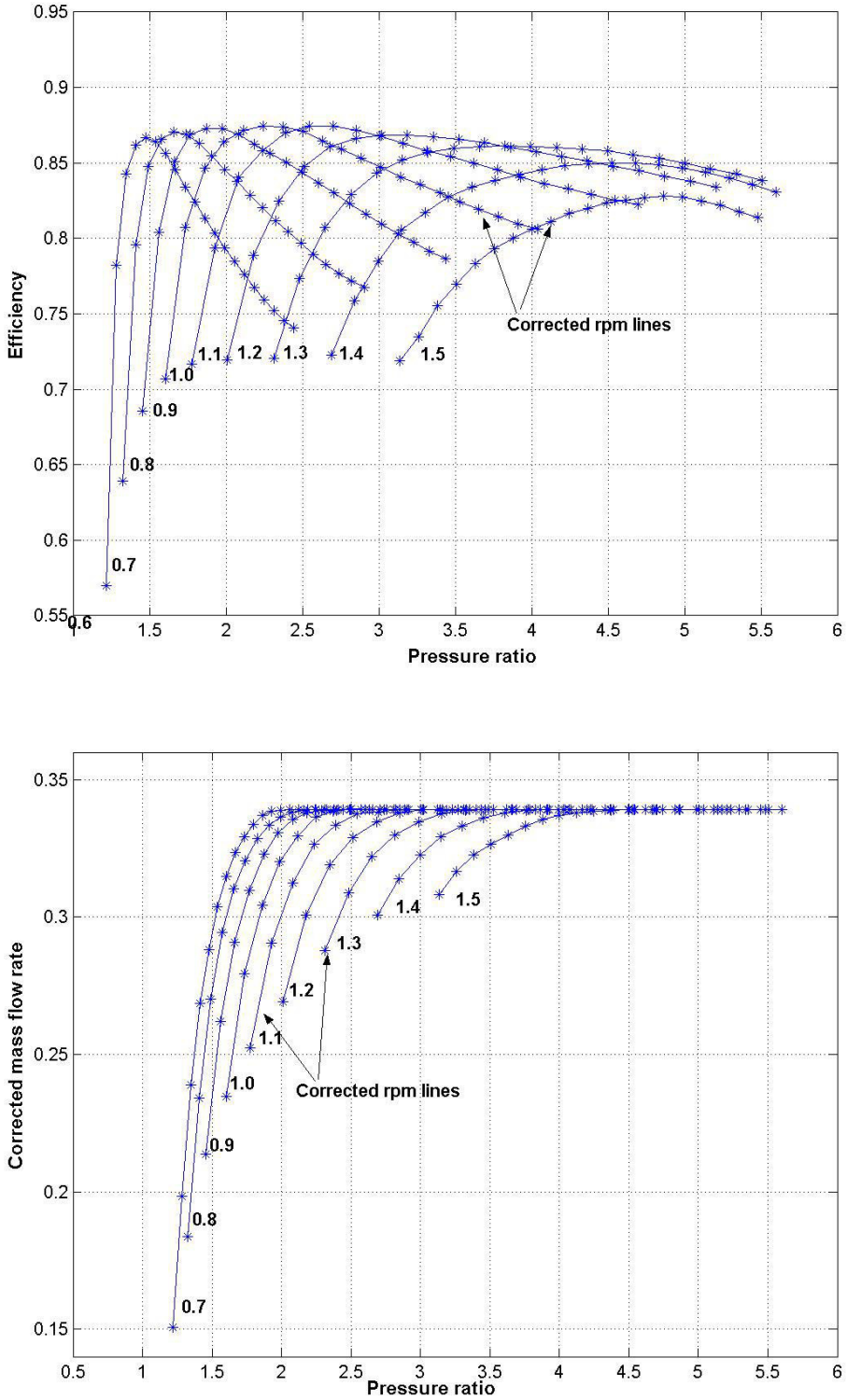

Figure 4-8 Performance Map of the Modeled Turbine, Based on the Radial Turbine Map NASA-CR-174646

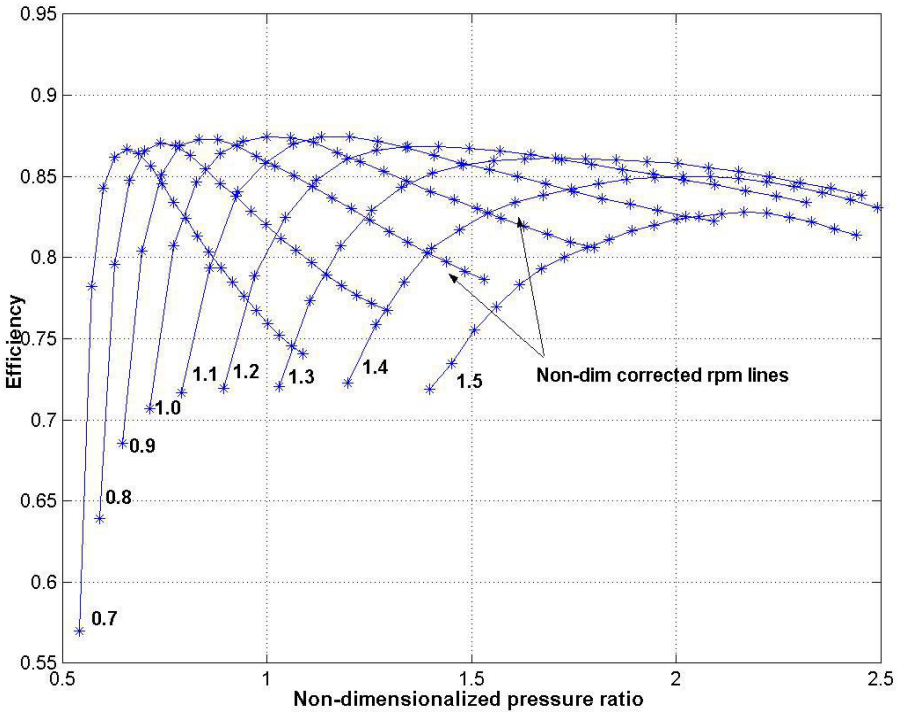

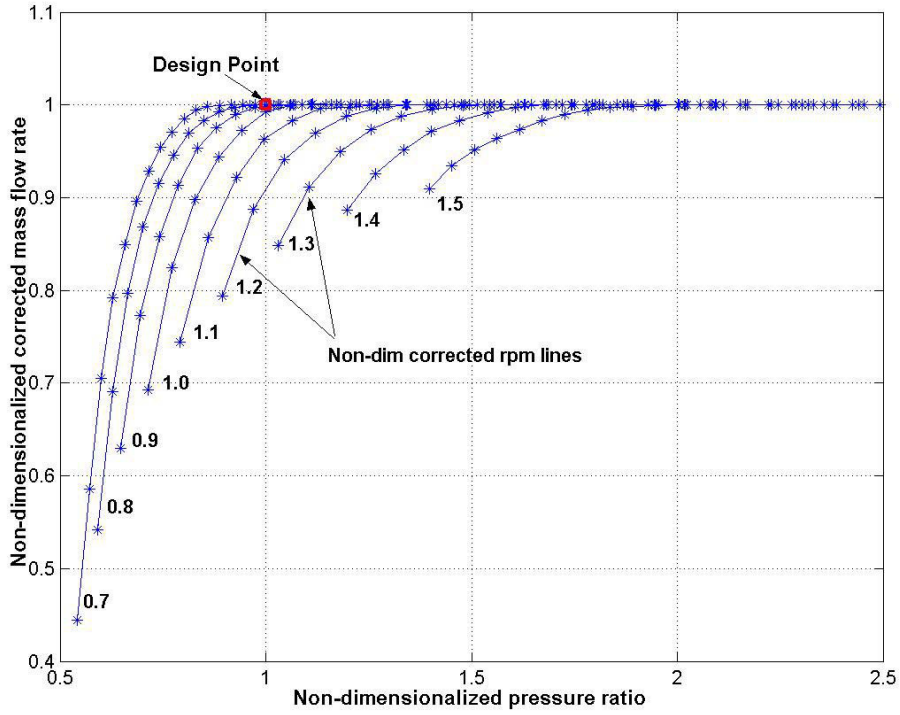

Figure 4-9 Normalized Performance Maps for NASA-CR-174646

4.6.4 TURBINE MODEL

The turbine model is similar to the compressor model. It uses overall thermodynamic relations to calculate the exit stream properties at off-design conditions. The model works under the same assumptions as mentioned for the compressor model. With the given inlet conditions, the operating point is located. The code implementing the maps outputs efficiency and mass flow rate for the given pressure ratio and rpm. The following equations are used to calculate the power and exit temperature.

$$\Delta h_{is} = Cp\left(T_{is} - T_i\right) \tag{4-54}$$

$$\Delta h_{is} = CpT_i\left(\frac{T_{is}}{T_i} - 1\right) \tag{4-55}$$

now, for an isentropic process,

$$\frac{T_{is}}{T_i} = \left(\frac{P_e}{P_i}\right)^{\frac{\gamma-1}{\gamma}} \tag{4-56}$$

hence, from the overall turbine efficiency definition,

$$\Delta h = \eta_T \Delta h_{is} \tag{4-57}$$

If, $\dot{m}_g$, is the gas flow rate in the turbine, then the turbine power is,

$$\dot{W}_C = \dot{m}_g \Delta h \tag{4-58}$$

The exhaust temperature is calculated using the actual enthalpy change as,

$$T_e = T_i + \frac{\Delta h}{Cp} \tag{4-59}$$

4.6.4 TURBINE COMPRESSOR MATCHING

The turbine that drives the compressor should be matched with the compressor at steady state. `Matching' means that the power and the rpm should be same for the compressor and the turbine. The typical way of matching is to use the shaft speed model, which balances the compressor, the turbine and the alternator power. The power that is still unbalanced goes to accelerate the turbine and the compressor until the steady state is reached. This technique requires the mass and moment of inertia of these components, which are unknown parameters in the current study. An alternative approach, developed by the author, is adopted here and has been shown schematically in figure 4-10.

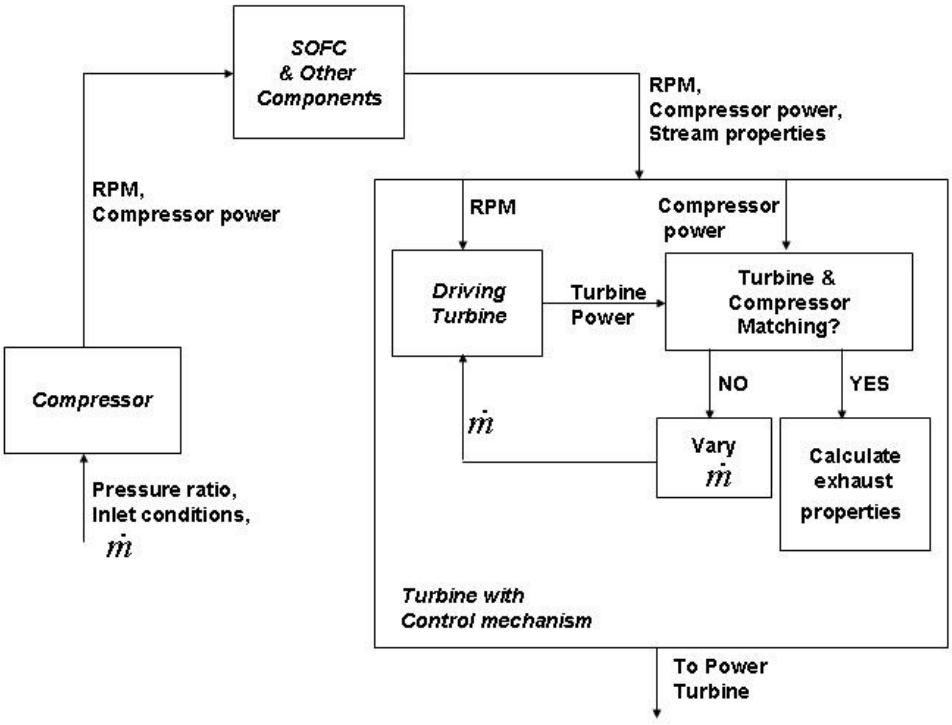

Figure 4-10 Turbine and Compressor Matching Methodology

If, $\dot{m}_g$, is the net mass flow rate, $\dot{m}_T$, is the mass flow going into the turbine, P_g is the pressure of the stream before entering the turbine, and P_T is the pressure of the stream coming out of the turbine, then the exhaust pressure can be calculated by using the law of partial pressures.

The stream exhaust pressure is,

$$P_e = \frac{(\dot{m}_g - m_T)P_g + \dot{m}_T P_T}{\dot{m}_g} \tag{4-60}$$

And the exhaust temperature is calculated as,

$$T_e = \left(\frac{\dot{m}_T P_e}{\dot{m}_g P_T}\right) T_T \tag{4-61}$$

where, T_T, is the temperature of the stream coming out of the turbine.

4.7 IMPLEMENTATION OF THE CODE

The model presented in this chapter is implemented in Matlab 6.5, which is a mathematical package suitable for solving a mixed system of differential, integral, and algebraic equations. The

Simulink toolbox of Matlab provides a graphical interface that is easy to understand and gives a virtual view of the actual hybrid system. The front end of the hybrid system is a Simulink graphical interface in which each component (i.e. SOFC, turbine, compressor etc) is represented by a virtual block with a set of codes either written in sequential language of Matlab or in the Simulink itself. The back end of the interface is set of files of data required or reusable programs by the Simulink.

5. CONFIGURATION SELECTION AND CYCLE ANALYSIS

As discussed in earlier chapters, selecting a configuration is one of the key steps before designing a hybrid system. This chapter presents various configurations of the SOFC/GT hybrid system and discusses why one configuration is better than the other. Once the optimum configuration is selected, a complete cycle analysis is presented. A design point for the cycle is chosen and then design and off-design performances are analyzed.

5.1 MODELING ASSUMPTIONS AND OPERATING CONDITIONS

- The model assumes that the cycle is running at design point until the optimum configuration is chosen.
- Pressures losses in the fuel cell, combustor, and piping are negligible
- The complete system is adiabatic i.e. no wall heat losses.
- The fuel pump power is not included while calculating the cycle efficiency.

The following are the operating conditions for the cycle components:

Compressor:

Polytropic Efficiency: 85%
Compression ratio: 2.9

Turbine:

Polytropic Efficiency: 88%
Pressure ratio: 2.9

Fuel composition: 97% H_2 + 3%H_2O by mol
Air composition: 21% O_2 + 79% N_2 by mol

SOFC:

Figure 5-1 shows the polarization curve reproduced in Matlab. A current density equal to 1 A/cm^2 is chosen as the operating point in the entire modeling.

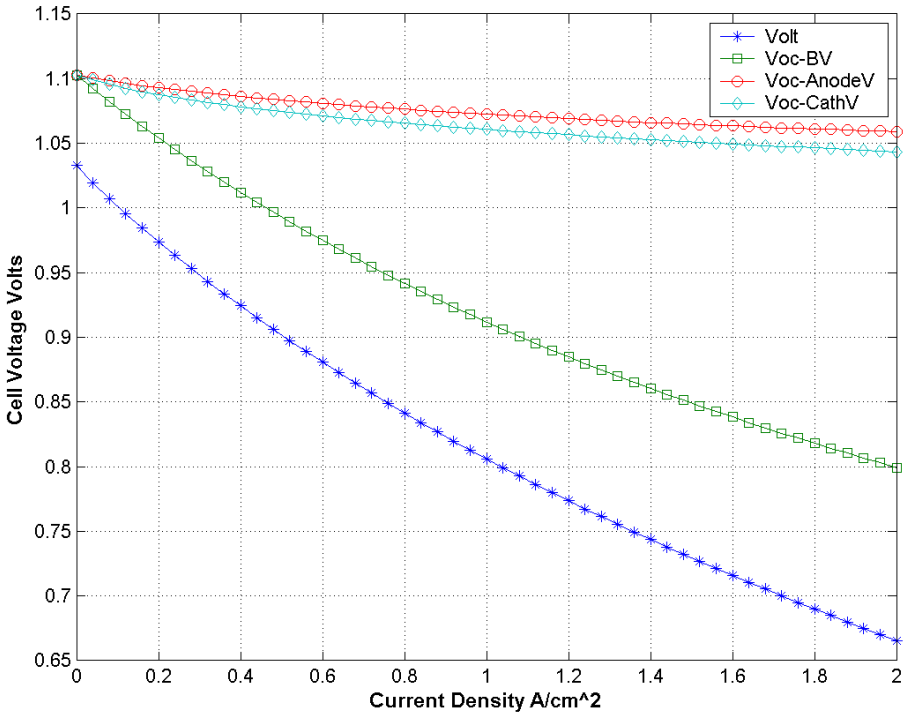

Figure 5-1 Polarization Curve of SOFC [PNNL, 2002]

Design condition

Sea level full power is taken as the design condition of the system. For aircraft applications, this choice is based upon the fact that the exhaust pressure at sea level is higher than the one at cruise altitude. In this way, the power extracted from the turbine will be less and to meet the power requirements the stack power needs to be higher. Higher stack power means higher heat and higher external cooling and thus higher air flow rate to the stack. Higher airflow rates require higher compressor power and higher turbine work. Therefore, the line of arguments suggests that sea level full power should be the design point. The fuel cell power is maximized at the design point. This design point selection and reasoning is taken from [CAPS, 2005].

Design Temperature: 25^0C
Design Pressure: 1 atm

5.2 CONFIGURATION SELECTION

Deciding upon the optimum configuration is one of the key steps in modeling a gas turbine hybrid system. In this work, a few configurations of the hybrid system are simulated and their performances are analyzed. Based upon the comparative study, the best configuration is chosen and discussed in detail. The basic parameters that are focused at, in choosing the optimum configuration, are the cycle efficiency and the fuel cell power.

5.2.1 CONFIGURATION 1: PROCESS DESCRIPTION

Figure 5-2 shows the schematic representation and Figure 5-3 shows the screen shot of the Matlab-Simulink model of the SOFC-GT Hybrid system configuration 1. Air is compressed and sent to the air heat exchanger. From the fuel pump, a compressed fuel stream (97% H_2 + 3% H_2O by mol) enters the fuel heat exchanger. The air and fuel heat exchangers are sequentially fed by the hot exhaust from the turbine (HPT). The exhaust from the turbine preheats the air and fuel streams.

After pre-heating, both the main streams of air and fuel enter (air at cathode and fuel at anode) the SOFC stack. From the heat exchangers, part of the preheated streams of air and fuel are bypassed to the combustor. The output of the fuel cell consists of electrical power and hot gasses. The hot exhaust is sent to combustor where it is burnt with additional fuel and air (from the bypassed streams). The hot exhaust is fully expanded to the ambient pressure and power is extracted to run the electrical generator. The exhaust form the turbine enters the air and fuel heat exchangers, respectively.

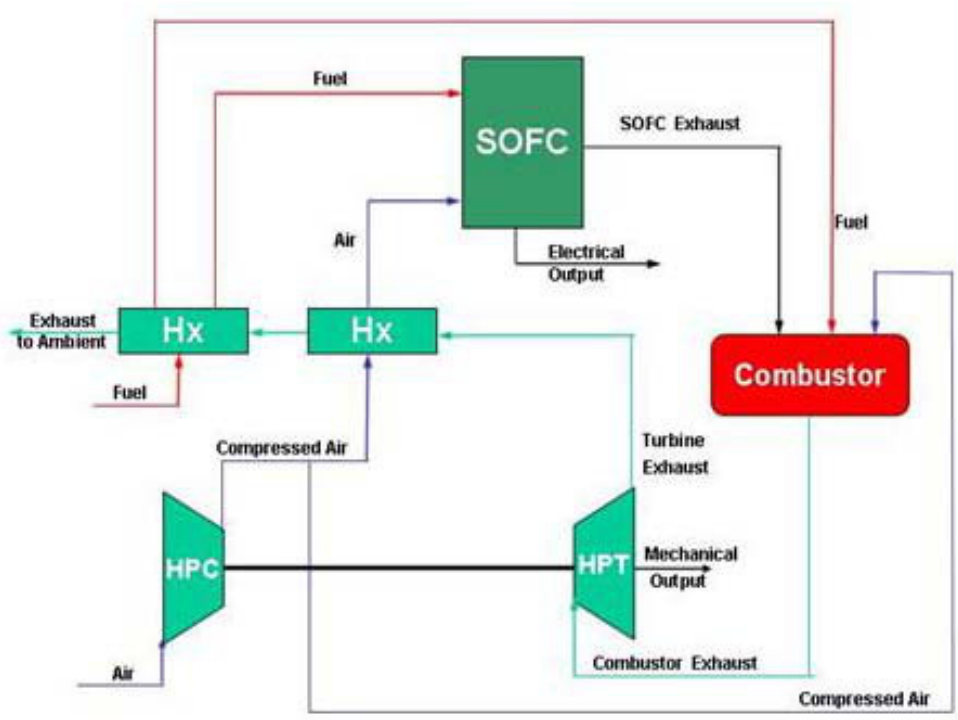

Figure 5-2 Schematic of Configuration 1

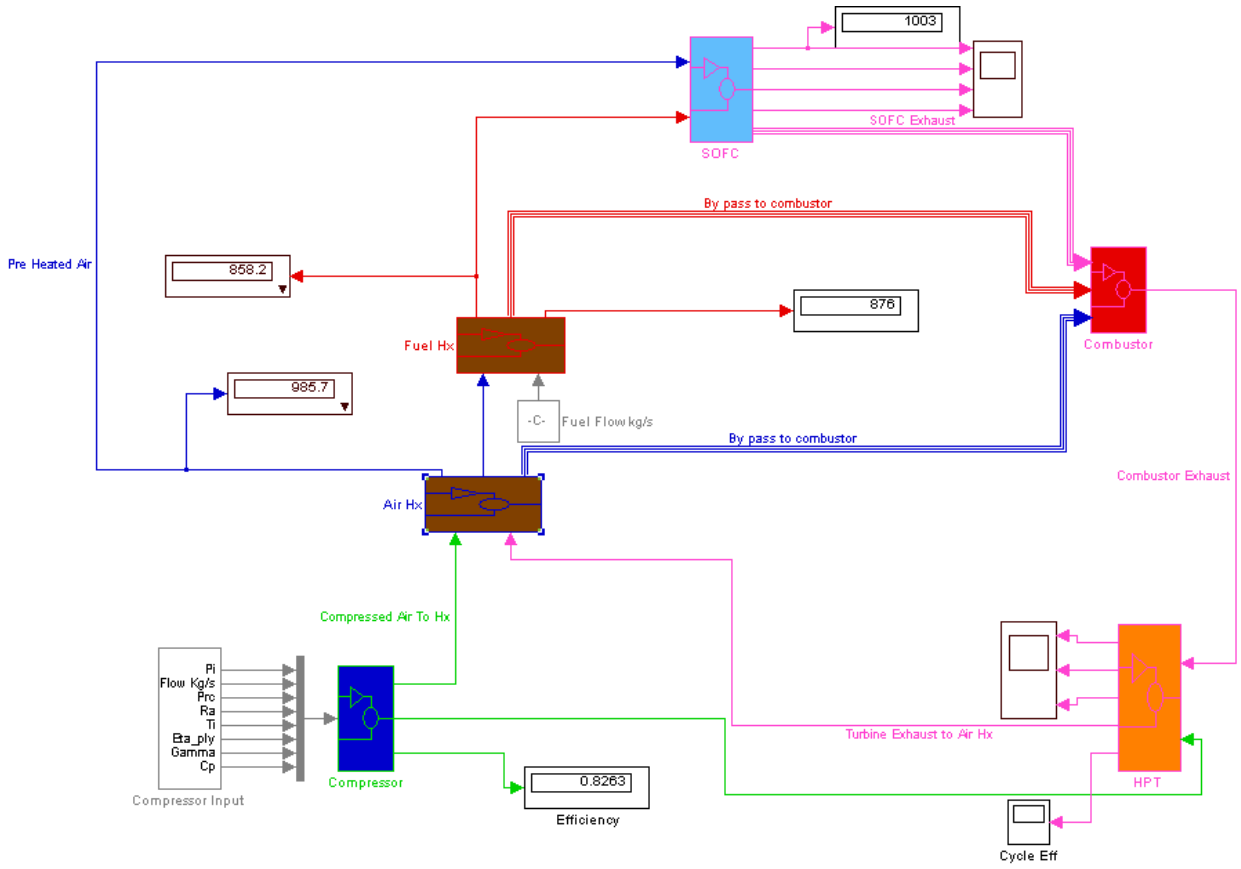

Figure 5-3 Working Simulink Model of SOFC-GT Hybrid System Configuration 1

5.2.2 CONFIGURATION 2A: PROCESS DESCRIPTION

Figure 5-4 & 5-5 show the second configuration analyzed. The difference between configuration 1 and configuration 2A is that in configuration 2A, there is no by pass stream from the air heat exchanger. Instead, soon after the compressor, one stream of compressed air is bypassed to the combustor. The reason why this is done, which turns out to be an improvement in the configuration, is discussed later.

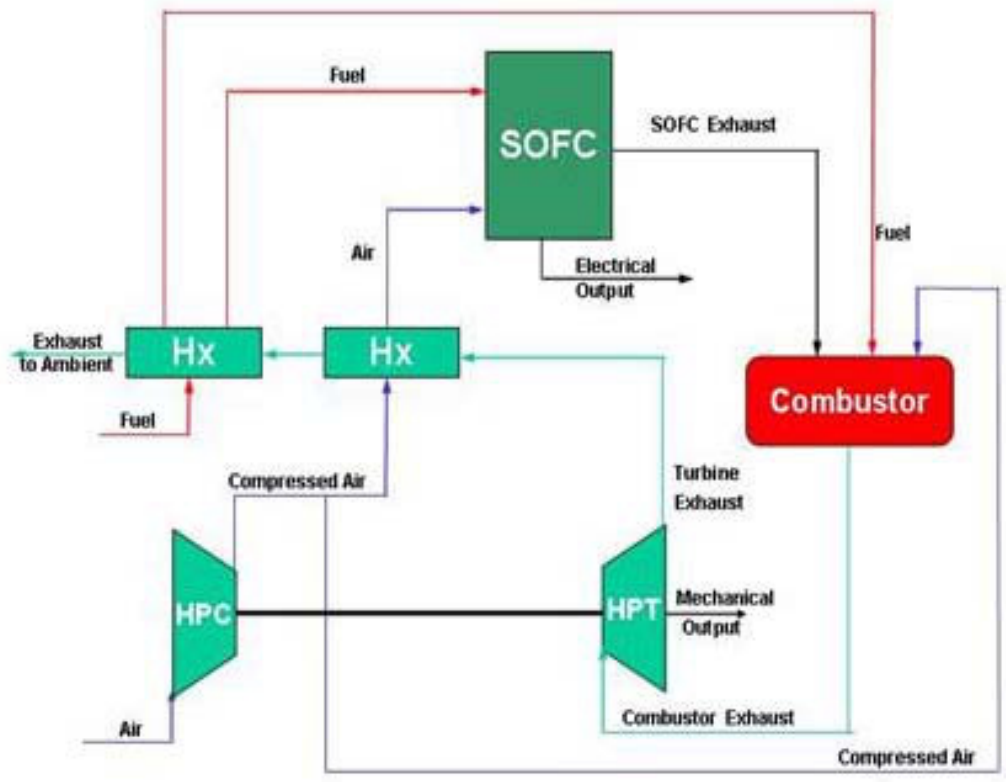

Figure 5-4 Schematic of Configurations 2A, 2B

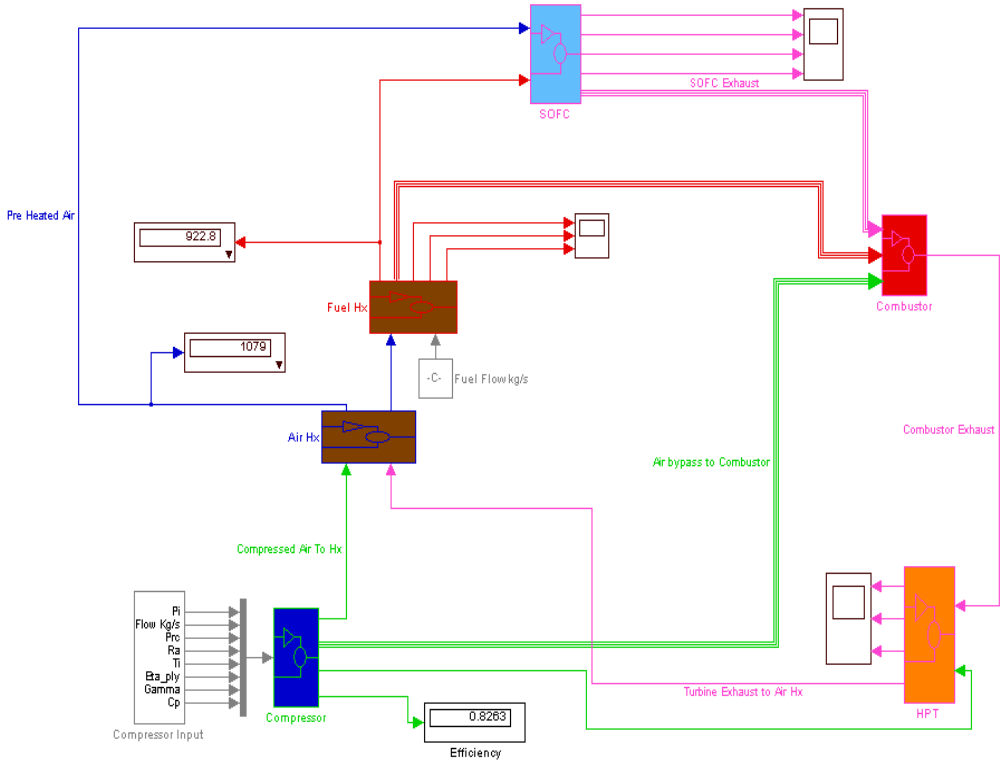

Figure 5-5 Working Simulink Model of SOFC-GT Hybrid system Configurations 2A, 2B

5.2.3 CONFIGURATION 2B: PROCESS DESCRIPTION

Configuration 2B is same as configuration 2A except by the fact that configuration 2B is using counter flow heat exchangers. All the configurations discussed previously use parallel flow heat exchangers. The need of using counter flow heat exchanger and advantages of configuration 2B over 2A are discussed in detail in the comparative study.

5.2.4 CONFIGURATION 3: PROCESS DESCRIPTION

Figure 5-6 and Figure 5-7 show the schematic and Simulink representation of configuration 3. All the compressed air is preheated by the turbine exhaust in the air heat exchanger and sent to the fuel cell. The fuel stream is heated by the hot cathode air coming out of the fuel cell and enters the anode of the SOFC. After exiting the fuel heat exchanger, the cathode air stream enters the combustor. The anode exhaust of the SOFC is sent to the combustor with additional fuel and cathode air from the fuel heat exchanger. The hot exhaust from the combustor is expanded in the turbine and mechanical power is extracted. Configuration 3 gives the best performance out of all the configurations considered in this study. The results are discussed in detail later.

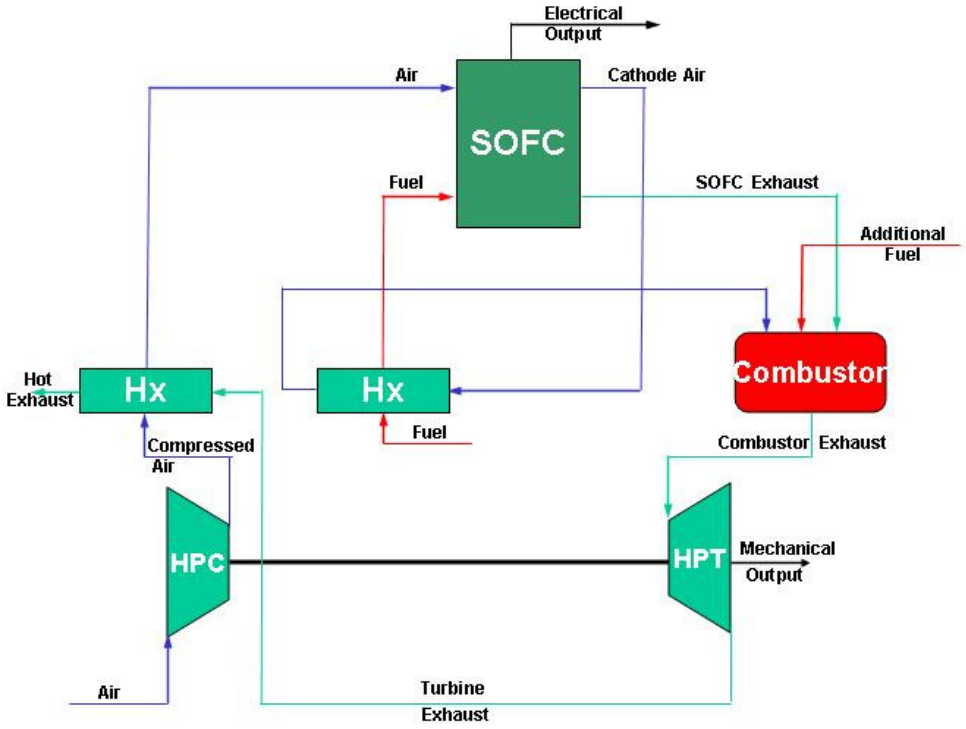

Figure 5-6 Schematic of Configuration 3

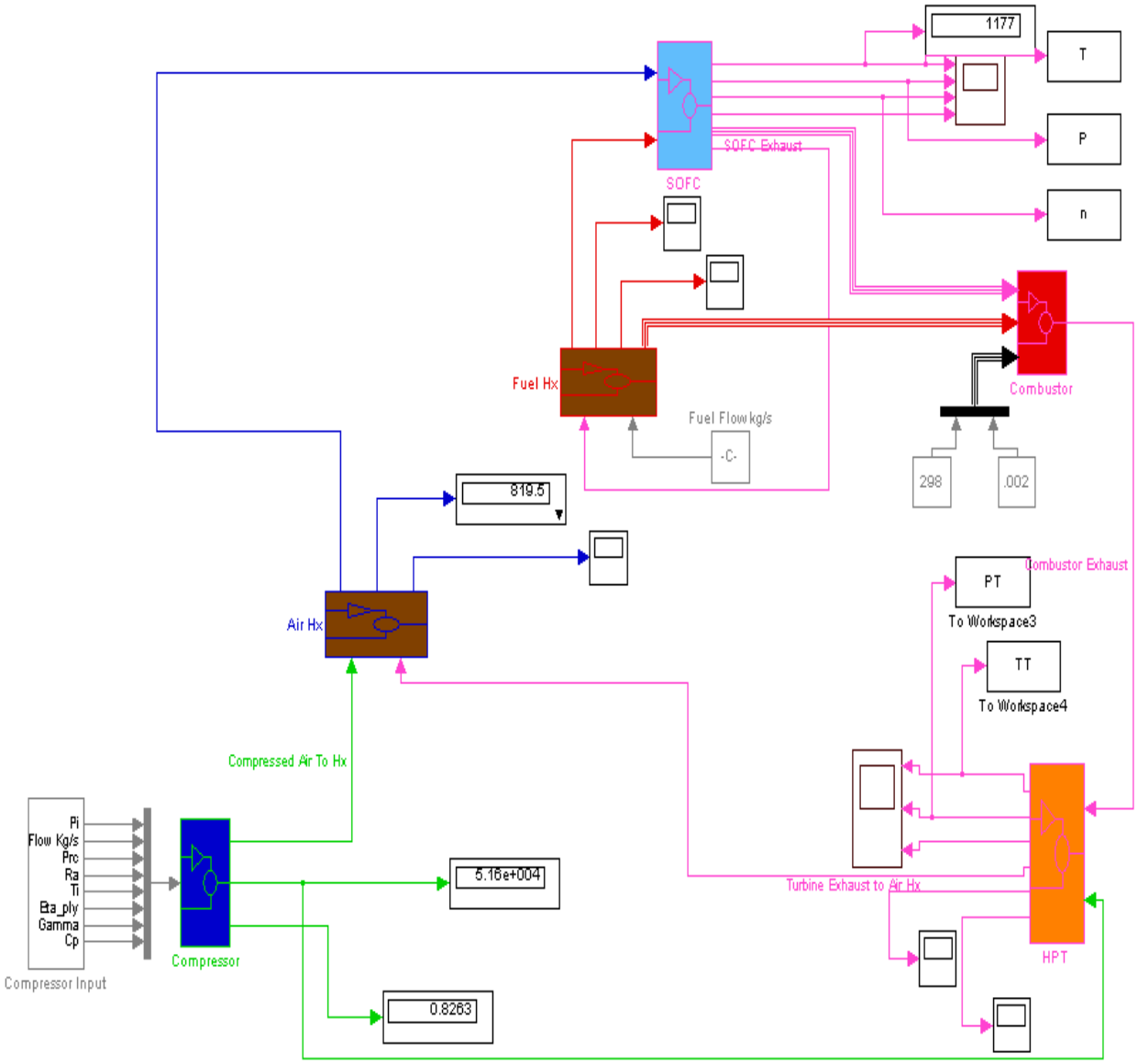

Figure 5-7 Working Simulink Model of SOFC-GT Hybrid System Configuration 3

5.3 COMPARATIVE STUDY

Table 5-1 presents the results for the configurations discussed above.

Table 5-1 Comparative Data for the four Configurations

	Configuration 1	Configuration 2A	Configuration 2B	Configuration 3
Fuel flow (g/s)	9.62	9.62	9.62	8.56
Air flow (g/s)	400	400	400	400
SOFC Temperature (^{0}C)	730	832	944	904
Turbine Inlet Temp (^{0}C)	1477	1136	1166	1378
SOFC power (kW)	237	330	351	333
HPT (kW)	144	104	108	130
Total power (kW)	381	434	459	463
Cycle efficiency	42 %	48%	51 %	58 %
Exhaust Temp(^{0}C)	603	670	617	546

From the Table 5-1, it can be seen that configuration 1 has the lowest performance and configuration 3 gives the best steady state performance. Configuration 1 gives only ~42% efficiency. We can say that the low performance of configuration 1 can be attributed to the low operating temperature of the fuel cell stack, as the SOFC performance is directly proportional to the operating temperature. Also, the turbine inlet temperature is exceeding the maximum allowable temperature (1400 ^{0}C). As we move from configuration 1 to 3, the operating temperature improves and hence the performance of the fuel cells.

Configuration 2A is an improved version of configuration 1. The entire stream coming out of the compressor is not sent to heat exchanger and preheated; instead air is bypassed to the combustor and only a partial stream enters the air heat exchanger. This change improves the stack operating temperature because of enough preheating. The efficiency reached is 48%. SOFC gives around 76% of the total power, which is a significant improvement from configuration 1.

Configuration 2B is same as configuration 2A except that configuration 2B is using counter flow heat exchangers. The performance of the SOFC is limited by its operating temperature. Low operating temperature is observed due to low preheating of fuel and air streams. Counterflow heat exchanger utilizes the hot stream's enthalpy in a more efficient manner and the performance of SOFC from 2A to 2B improves (efficiency 51%).

The configuration 3 is chosen as the best configuration out of the configurations studied. Since not very high temperatures are required at the turbine exit, due to the high efficiency of the counterflow heat exchangers, the cathode air is utilized to preheat the fuel stream. After preheating the fuel stream, the cathode stream is circulated back to the combustor. The compressed high temperature exhaust from the combustor is expanded in the turbine. The enthalpy of the exhaust leaving the turbine is high enough to give the required preheating to the air stream in the air heat exchanger. The exhaust from the air heat exchanger is released to the ambient. The efficiency obtained in this case is 58% and the power of the fuel cell is around 72% of the total power. The turbine inlet temperature is also within the limits and exhaust temperature is lower than the other configurations.

The data for configuration 2B and configuration 3 give an impression that if heat exchanger's overall heat transfer is changed, there might be a case when configuration 2B can give better performance than configuration 3. Considering this, configuration 2B is further analyzed and Figure 5-8 shows the results in a graphical form.

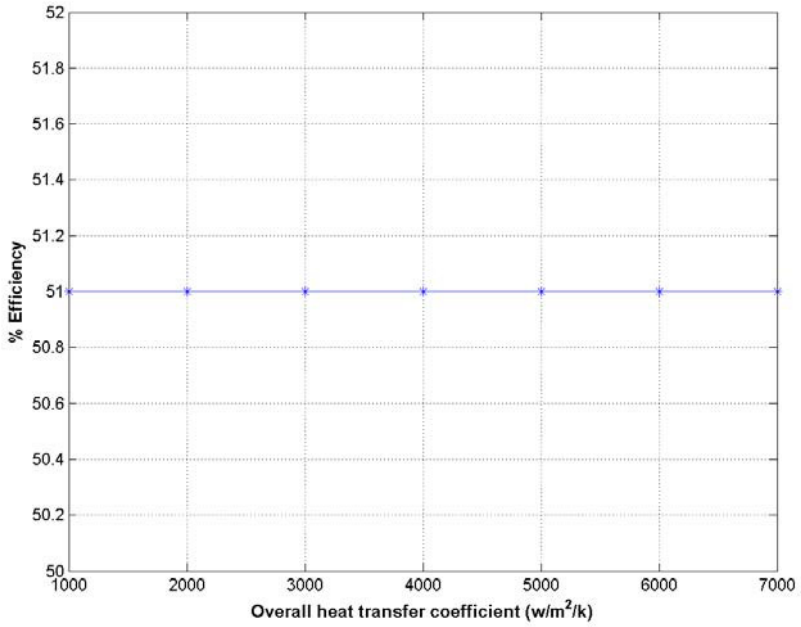

Figure 5-8 Sensitivity of Configuration 2B with respect to the Air Heat Exchanger's Overall Heat Transfer Coefficient

As it can be seen the efficiency of configuration 2B is not changing as the overall heat transfer coefficient is changed (the mass flow rate is constant and equal to 400 g/s). The reason for this behavior, is that even at the minimum heat transfer coefficient, the heat exchanger is operating at maximum effectiveness and is allowing the maximum heat transfer. Also, at a particular heat transfer coefficient when the mass flow rate is increased, the efficiency of the cycle is found to be dropping for the configuration. This excludes the possibility of choosing the configuration 2B as the optimum one.

5.4 SENSTIVITY STUDY OF CONFIGURATION 3

Table 5-2 Data for Configuration 3 for Different Heat Transfer Coefficients and Air Mass Flow Rates

Heat exchanger overall heat transfer coefficient = 1000 w/m^{2}K					
Air flow(kg/s)	*Stack temp.(K)*	*cycle efficiency*	*Turbine inlet temp(K)*	*Exhaust temp(K)*	*Heat exchanger effectiveness %*
0.4	1177	57.8	1651	819.5	78.5
0.45	1031	50	1489	759	75
0.5	921	36.5	1359	714	71.6
0.55	Stack temp<600 ^{0}C				
0.6					
0.65					
Heat exchanger overall heat transfer coefficient = 2000 w/m^{2}K					
Air flow(kg/s)	*Stack temp.(K)*	*cycle efficiency*	*Turbine inlet temp(K)*	*Exhaust temp(K)*	*Heat exchanger effectiveness %*
0.4	1550	60	1959(forbidden)	851	92
0.45	1364	61.2	1764(forbidden)	777	90
0.5	1210	60.7	1599	720	87.4
0.55	1084	56.2	1462	677	85
0.6	983.8	47	1348	643	82.6
0.65	901	35	1253	617	80.5
0.7	834	14	1173	598	78.5
Heat exchanger overall heat transfer coefficient = 3000 w/m^{2}K					
Air flow(kg/s)	*Stack temp.(K)*	*cycle efficiency*	*Turbine inlet temp(K)*	*Exhaust temp(K)*	*Heat exchanger effectiveness %*
0.4	Forbidden				
0.45					
0.5					
0.55	1247	62.5	1601	684	92
0.6	1129	60	1473	645.4	90
0.65	1030	53.2	1365	615	88.2
0.7	948	43.5	1272	591.5	86.5
Heat exchanger overall heat transfer coefficient = 4000 w/m^{2}K					
Air flow(kg/s)	*Stack temp.(K)*	*cycle efficiency*	*Turbine inlet temp(K)*	*Exhaust temp(K)*	*Heat exchanger effectiveness %*
0.4	Forbidden				
0.45					
0.5					
0.55					
0.6	1230	63.2	1560	650	94
0.65	1124	60.5	1445	617	92.5
0.7	1033	54.2	1346	590	91

Table 5-2 continued

Heat exchanger overall heat transfer coefficient = 5000 w/m^{2}K					
Air flow(kg/s)	*Stack temp.(K)*	*cycle efficiency*	*Turbine inlet temp(K)*	*Exhaust temp(K)*	*Heat exchanger effectiveness %*
0.4	Forbidden				
0.45					
0.5					
0.55					
0.6	1297	64.4	1618	654.4	96.3
0.65	1190	63.3	1503	619.5	95.2
0.7	1096	59.8	1401	591.5	93.9
Heat exchanger overall heat transfer coefficient = 6000 w/m^{2}K					
Air flow(kg/s)	*Stack temp.(K)*	*cycle efficiency*	*Turbine inlet temp(K)*	*Exhaust temp(K)*	*Heat exchanger effectiveness %*
0.4	Forbidden				
0.45					
0.5					
0.55					
0.6	1342	65	1657	658	97.6
0.65	1237	64.5	1544	622	96.7
0.7	1142	62.4	1441	593	95.8
Heat exchanger overall heat transfer coefficient = 4000 w/m^{2}K					
Air flow(kg/s)	*Stack temp.(K)*	*cycle efficiency*	*Turbine inlet temp(K)*	*Exhaust temp(K)*	*Heat exchanger effectiveness %*
0.4	Forbidden				
0.45					
0.5					
0.55					
0.6					
0.65	1269	65	1572	624	97.8
0.7	1176	63.8	1471	594	97
0.71	1159	63.3	1452	588	96.9
0.75	1092	60	1380	570	96.2

Table 5-2 shows the data for configuration 3 at different mass flow rates for varying overall heat transfer coefficients (UA). 'Forbidden' means that a particular condition is not permissible as the maximum allowable turbine inlet temperature is 1400^0C. As we move from low UA to high UA, the 'forbidden' operating condition shifts to the higher mass flow rates. Figure 5-9 shows this variation in a graphical form.

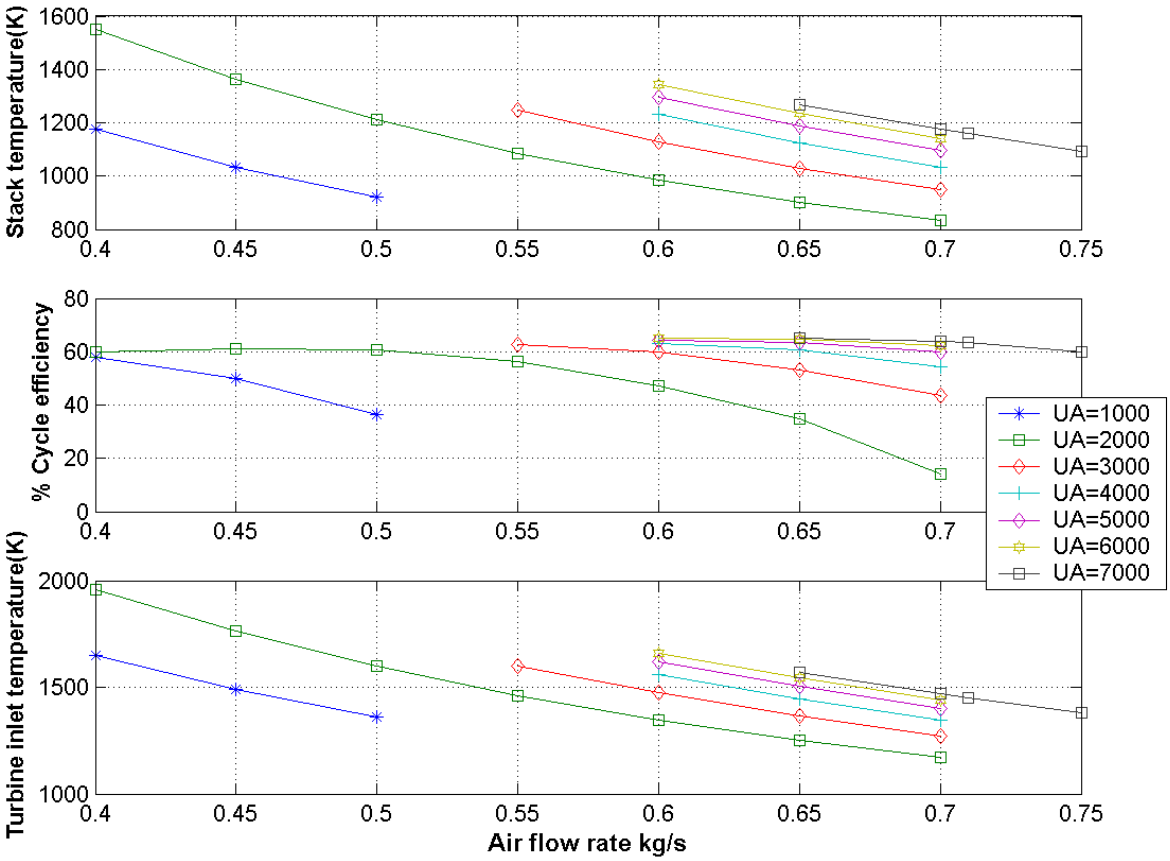

Figure 5-9 Configuration 3 Sensitivity Study

The efficiency plot shows that at UA=7000 w/m^{2}K, the cycle efficiency becomes more or less insensitive to the change of mass flow rate. When the mass flow changes from 0.65 to 0.75, efficiency changes from 65 % to 60% but the stack temperature and turbine inlet temperature improve significantly.

An overall heat transfer coefficient of, UA = 7000 is used later to compare configuration 3 with [Freeh, 2005] and [Steffen, 2005].

5.5 IMPROVED CONFIGURATION 3: DESIGN AND OFF-DESIGN PERFORMANCE

From the previous analysis we have fixed the configuration and the components specifications. So far configuration 3 is based on the simplified compressor and turbine models. The models are now modified to include turbine and compressor maps. The improved model of configuration 3 uses performance maps for a real compressor (DLR radial) and turbine (NASA-CR-174646). To calculate the design and off-design performance of the configuration, a steady state model of the SOFC is developed. One more difference between base configuration 3 and its improved version is that in the latter configuration, the turbine is split into a driving and a power turbine. The reason

being that the compressor and the driving turbine need to be matched. Figure 5-10 shows the working Simulink model of the improved configuration-3.

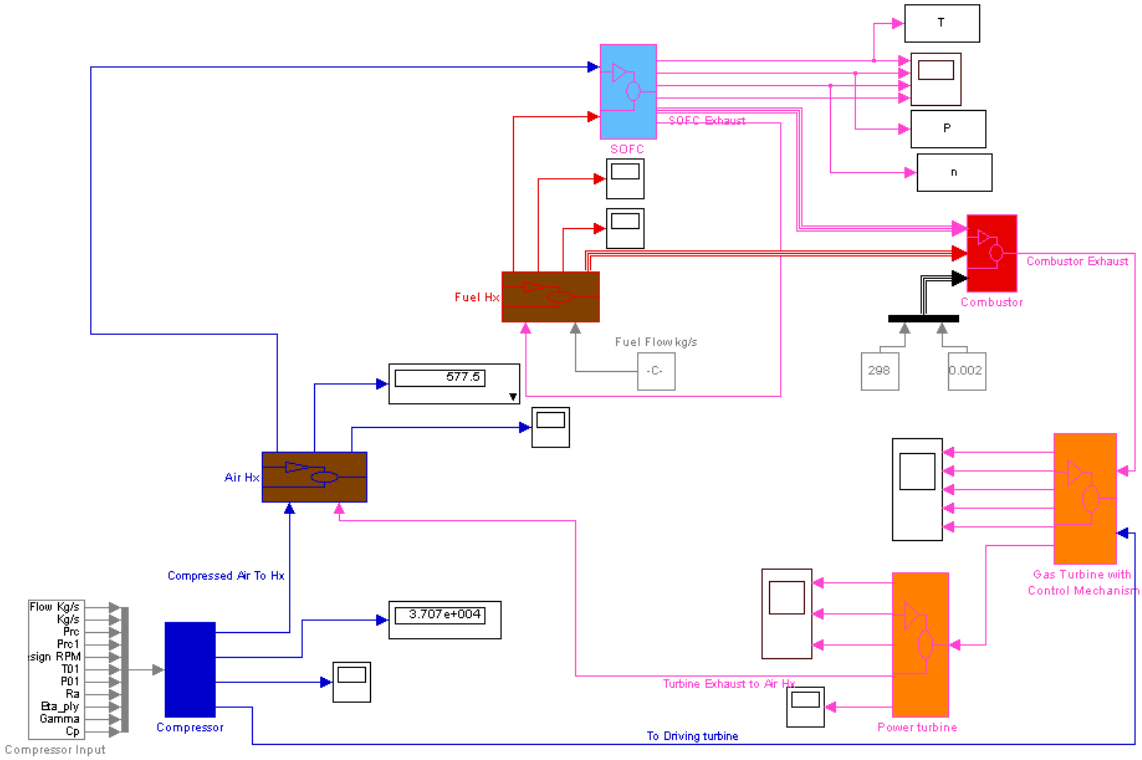

Figure 5-10 Simulink Model of Improved Congfiuration-3

One important point to be noted is that the analysis henceforth will use some adjustable parameters (compressor mass flow rate, pressure ratio) in order to simulate the same conditions as [CAPS, 2005]. The parameters used are:

Compressor: DLR radial

Inlet temperature: 298 K
Inlet pressure: 101325 Pa
Design mass flow rate: adjustable
Design pressure ratio: 2.88

Air heat exchanger:

Counter flow
Overall heat transfer coefficient (UA): 7000 w/m^{2}K

Fuel heat exchanger:

Counter flow
Overall heat transfer coefficient (UA): 360 w/m^{2}K

Driving Turbine: NASA-CR-174646

Design mass flow rate: adjustable
Design pressure ratio: 1.5

Power Turbine: NASA-CR-174646

Design mass flow rate: adjustable
Design pressure ratio: 2

5.5.1 PERFORMANCE ANALYSIS

DESIGN PERFORMANCE: SEA LEVEL

Table 5-3 shows the results of improved configuration 3 and reference [CAPS, 2005]. The parameters shown in *italics* are adjustable parameters and are varied in the model in order to compare the performance with the reference case.

Table 5-3 Design Performance of the Model and the Reference [CAPS, 2005]

	Configuration-3	**Reference [CAPS, 2005]**
SOFC net power	315 kW	429 kW
Turbine power	138 kW(mechanical)	19 kW(electrical)
Cycle efficiency	56.5%	42%
Stack pressure	*2.9 bar*	*2.9 bar*
Stack temperature	*856 ^{0}C*	*850 ^{0}C*
Compressor inlet pressure	*14.7 psia*	*14.7 psia*
Compressor pressure ratio	*2.88*	*2.88*
Compressor efficiency	85%	83%
Turbine outlet pressure	*17.1 psia*	*17.1psia*
Turbine Pressure ratio	2.47	2.37
Turbine efficiency	87%	84%

The results show that the model is giving better sea level performance than [CAPS, 2005]. The efficiency observed for the model is 56%, which is nearly 33% more than the reference case. The SOFC power is nearly 70% of the total power while this percentage is nearly 96 in the reference case.

OFF-DESIGN PERFORMANCE: CRUISE

Table 5-4 Off-design Performance of the Model and the Reference [CAPS, 2005]

	Configuration 3	**Reference [CAPS, 2005]**
SOFC net power	304	279
Turbine power	273	161
Cycle efficiency	72%	73%
Stack pressure	*1.36*	*1.3*
Stack temperature	*848^0C*	*837^0C*
Compressor inlet pressure	*10.9 psia*	*10.9 psia*
Compressor pressure ratio	*1.83*	*1.83*
Compressor efficiency	69%	75%
Turbine outlet pressure	*3.2 psia*	*3.2 psia*
Turbine Pressure ratio	6.23	6
Turbine efficiency	*82%*	*88%*

In case of off-design operation, the efficiencies are found to be similar. The SOFC power is 53% of the total power (reduced from 68% in the design case). For the reference case this percentage changes from 96% to 63%. At sea-level, the driving unit is the SOFC where as at cruise, the SOFC power reduces and almost 50% power is coming from the turbine.

Figure 5-11 shows the performance of the turbine and the compressor at design and off design conditions. As mentioned earlier in this chapter, sea level condition requires more mass flow rate through the compressor and the fact can be verified with the compressor performance map. The turbine operates at high expansion ratio at cruise condition and delivers more power compared to the sea level condition. Though the turbine and the compressor are giving more of less the same performance in both the author's work and the reference, the SOFC performance is not comparable. The difference can be attributed to the fact that the model used in the current study is not very flexible and needs current density or operating voltage as an input. In a real hybrid system, current density is not a controllable parameter. There are some important points to be emphasized here as mentioned in chapter-3, current modeling is an effort to simulate a hybrid system in Matlab and gives an insight to the reader that the results are inline with [CAPS, 2005] but the model has to be improved on many aspects (discussed later) before it can actually be compared with the reference. The scope of improvement has been discussed in the later part of the thesis.

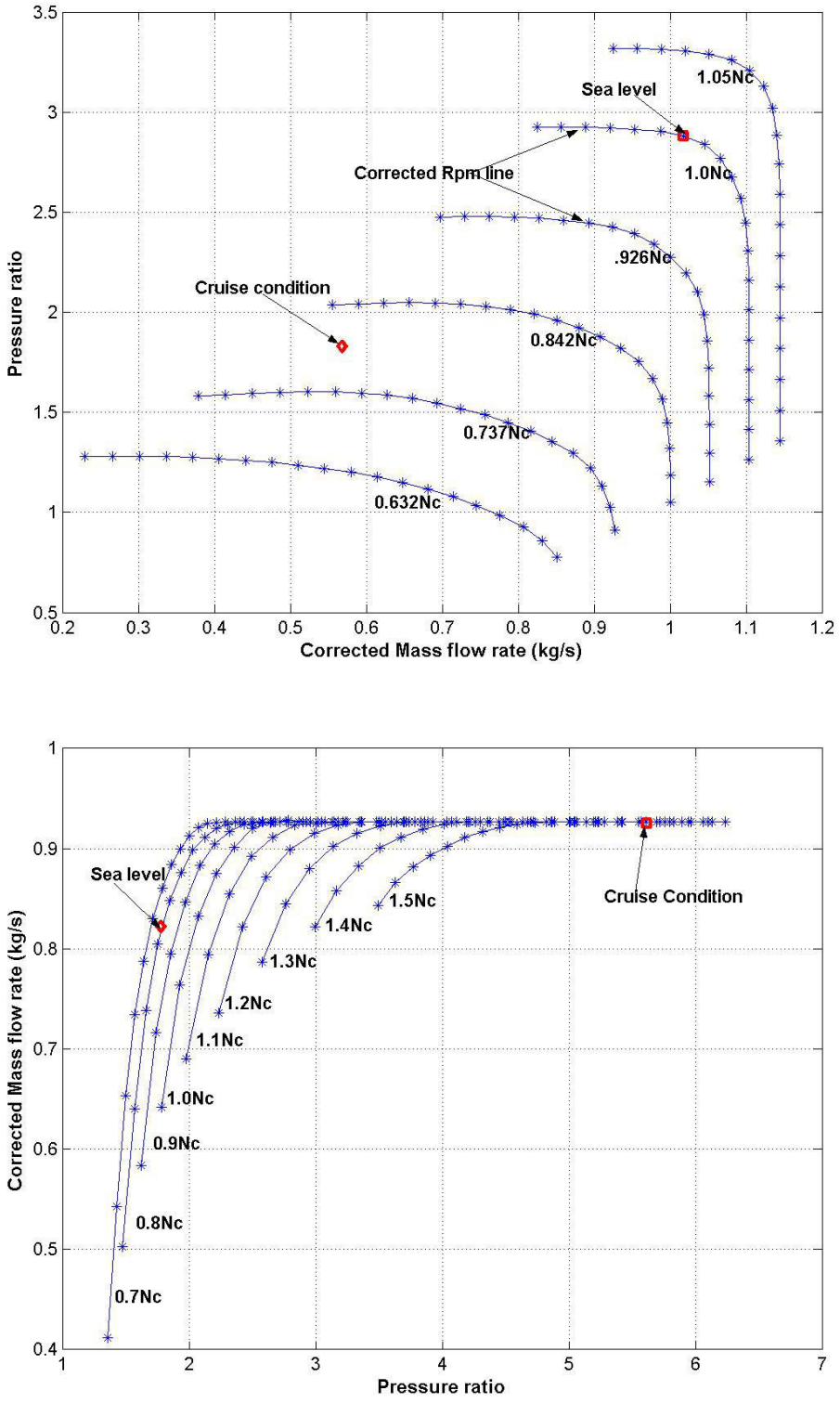

Figure 5-11 Compressor (above) and Turbine (below) Performances at Seal Level and Cruise Conditions

6. CONCLUSIONS AND FUTURE DIRECTIONS

6.1 CONCLUSIONS

In this work a hybrid SOFC/GT system model is developed and implemented in Matlab-Simulink. A single button cell SOFC model developed at PNNL [PNNL, 2002] has been extended to the Stack model and integrated with a hybrid system.

Two types of models have been developed for compressors and turbines. One based on simple thermodynamic expressions and a more realistic one based on the performance maps. The simple models are used in the preliminary part of the study to select among several configurations, the one with highest overall efficiency. The compressor maps are later introduced into the selected configuration. The compressor and turbine matching is done by the approach developed by the author (Figure 4-10) as the typical way (shaft speed model) requires the mass moment of inertia of the components.

Some important observations are made during the configuration selection. It is observed that parallel flow heat exchangers are not suitable for the hybrid systems as the exhaust temperature is required to be minimum. The counter flow heat exchanger utilizes the enthalpy of the stream in a better sense and is used in the configuration 2B and 3.

Some important observations are made by means of a sensitivity study of the whole cycle for the base configuration. The fuel cell performance is found to be a strong function of operating temperature (which depends upon the preheating of the input streams) and hence when the heat exchanger properties are varied with the air mass flow rate, the cycle performance shifts towards favorable conditions. The parameters that limit the cycle performance are the SOFC temperature, the turbine inlet temperature, and the exhaust temperature. Though at high SOFC temperatures, the cycle efficiency is high, the cycle operation under these conditions is not feasible after a certain point.

The base configuration is improved by implementing the performance maps of compressor and turbine in order to test the design and off-design performance of the cycle. The design and off-design conditions are compared to [CAPS, 2005], a study which is the main motivation of author's work.

The important fact found was that the base configuration, though not as comprehensive as used in the references, more or less gives the similar performance. At sea level conditions, driving unit of the system is fuel cell as 70% of the total power is coming from the SOFC and rest from the power turbine. The efficiency of the modeled system is found to be more than the reference case. At off design conditions, turbine gives more power and the percentage break-up of SOFC and turbine power is 53%-47%. In the reference case the same break up is 63%-37% but further modifications are required in the base configuration before both the systems can actually be compared.

6.2 FUTURE DIRECTIONS

The author's work is an attempt to model a basic hybrid system, which is in line with ongoing work at NASA Glenn Research Center. Before mentioning the scope of improvements, it is important to restate the assumptions that have been made while modeling the hybrid system:

1. All the pressure losses are assumed to be negligible.
2. A constant current density is assumed through out the analysis.
3. The driving turbine and compressor are not matched in a conventional way since the mass and geometrical distribution of both of them is unknown while doing the preliminary analysis.
4. Hydrogen is used as a fuel and hence internal reforming and desulphurization have not been incorporated.
5. The combustor of the model is based on simple combustion reactions and does not include the actual chemistry of the reaction.

Now, we can go through each of the above mentioned assumptions one by one. The first assumption is that the system assumes no pressure loss anywhere which can be considered a reasonable assumption for preliminary modeling but there are many factors which contribute to the system pressure loss such as losses in the piping due to surface roughness, losses in the flow channels of the fuel cell and combustion losses. All of these losses can be approximately accounted for by doing the statistical study of the available literature. Going to the second assumption, the SOFC model used in the system is a lumped mass model and both the voltage and the current density are unknowns. Except for the fuel flow rate, the only other controlling parameter is the external load, which has not been included in the presented modeling, and hence a constant current density is assumed in the entire analysis. Either an improved model of SOFC needs to be used or an external load condition has to be simulated in order to accurately predict the operating point of the fuel cell (i.e. current and density). The turbine-compressor matching has not been done by using the conventional shaft speed model. The shaft speed model balances the net power of the turbine with the power of the generator and the compressor at steady state. Until the steady state, the excess power goes in accelerating the compressor, the turbine and the generator. This model calls for the mass moment of inertia of the components to calculate the steady state rpm of the system. So far the mass of the components of the system is unknown and hence the conventional model could not be employed. Nevertheless, by using the preliminary specifications of the turbine and the compressor, a statistical study can be carried out to choose from existing compressors and turbines. Also, once the mass of all the components is known, transient analysis can be done for the entire system which is possible only for the SOFC as of now. The entire analysis has been done for hydrogen fuel but in practical cases '*Jet-A'* fuel is used for APU applications. In order to modify the system for the Jet fuel, an internal reformer and a desulphurizer needs to be integrated with the system simulating the entire chemistry of the reactions taking place. The package suggested for modeling the chemical reactions has been mentioned in [CAPS, 2005]. And the last assumption is that the combustor used in the system is based on simple combustion reactions and might not be actually simulating the chemical reactions occurring at the high operating temperatures. The package suggested in [CAPS, 2005] can be used to model the chemical reactions of the combustor.

The above discussion shows that modeling a hybrid system is an iterative process and has to be tested and retested before it can come close to a real system. The model presented in this thesis gives a starting point of that developmental process and leaves a lot of scope for future work in this direction.

APPENDIX

THE PNNL BUTTON CELL MODEL

A.1 STRATEGY & ASSUMPTIONS

1. The operating temperature is homogeneous over the entire unit button cell.
2. The gas composition is homogenous over the entire active area.
3. The model is physics-based and empirically calibrated.
4. The fuel and air streams experience a two degree change in temperature from inlet to exit.

A.2 INPUT PARAMETERS

1. Cell material properties and dimensions

Table A-1 Cell Material Properties and Dimensions

Component	*Thickness, μ mm*	*% Porosity*	*Tortuosity*
Electrolyte	10	NA	NA
Anode	600	30	2.50
Interconnect	0	NA	NA
Cathode	50	30	2.50

Active cell area = 3.8 cm^2

Table 4-1 presents the dimensions and properties of the single unit button cell. The terms used in the table are defined below:

Porosity: The porosity describes the void fraction of the medium, and is defined by the ratio[Bejan, 1995]:

$$\phi = \frac{V_p}{V_m}$$

where V_p is the non-solid volume (pores and liquid) and V_m is the total volume of the material, including the solid and non-solid parts. The porosity is a fraction between 0 and 1, typically ranging from less than 0.01 for solid granite to more than 0.5 for peat and clay.

Tortuosity: The tortuosity of a porous medium is a measure of the complexity of the flow path. It is the ratio of average length of the flow paths to the thickness of the medium.

2. Operating conditions

	Anode Stream	%	*Cathode stream*	%

Total Anode Fuel Flow : 200 sccm	H2	97.0	O_2	21.0
Total Cathode Air Flow: 300 sccm	CO	0.0	N_2	79.0
	H2O	3.0		
	CO2	0.0		
Operating pressure: 1 atm	N2	0.0		
Fuel inlet temperature: 1072 K Air inlet temperature: 1072	Total	100.0	Total	100.0

A.3 MODELING CALCULATIONS

The modeling calculations are done for a given current, material properties, and operating conditions under the mentioned assumptions.

1. CHEMICAL CALCULATIONS

With the given current density, *i*, the rate of oxygen transport is calculated and thus, the rate of fuel consumption:

Oxygen flux through electrolyte: $J_{O_2} = \frac{i}{4F}$ (A-1)

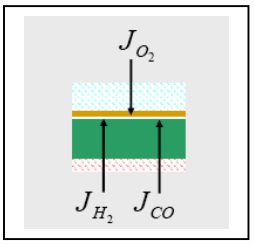

And, $J_{H_2} + J_{CO} = 2.J_{O_2}$ (A-2)

The product fluxes are opposite to reactant fluxes:

$$J_{H_2O} = -J_{H_2}$$
$$J_{CO_2} = -J_{CO}$$ (A-3)

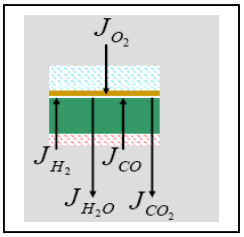

but still the ratio of H_2 oxidation to CO oxidation is unknown.

It is assumed that fuel gas is always in equilibrium with respect to the water gas shift reaction. This assumption is valid because the water gas shift reaction is highly active at high operating temperatures,

$$CO + H_2O \Leftrightarrow CO_2 + H_2$$ (A-4)

The equilibrium constant of the shift reaction is calculated by first calculating the free energy change of formation of the species:

$$Keq = \frac{[CO].[H_2O]}{[CO_2].[H_2]}$$ (A-5)

$$Keq = \exp\left(\frac{-\Delta G_{form,CO} - \Delta G_{form,H_2O} + \Delta G_{form,CO_2}}{RT}\right) \quad \text{(A-6)}$$

where,

$$\Delta G_{form,j} = \Delta H_{0,j} + A_j.T.\log T + B_j.T^2 + C_j / T + D_j T \quad \text{(A-7)}$$

$\Delta H_{0,j}$ is the heat of formation of the j^{th} species, and A, B, C, and D are constants taken from the CRC hand book of chemistry and physics.

Once K_{eq} is known, the equilibrium concentration of all the species at the inlet is calculated by solving system of equations (A-8 to A-16).

The following variables are defined in terms of the initial concentrations:

Let, $$V = [CO].[H_2O] \quad \text{(A-8)}$$

$$W = [CO] + [H_2O] \quad \text{(A-9)}$$

$$X = [CO_2].[H_2] \quad \text{(A-10)}$$

$$Y = [CO_2] + [H_2] \quad \text{(A-11)}$$

Then, $$K_{eq,T} = \left(V - SW + S^2\right) / \left(X + SY + S^2\right) \quad \text{(A-12)}$$

Here, S, represents the moles of H_2 created by the shift reaction and is solved from the quadratic equation, using the positive root.

$$[CO]_{eq} = [CO]_{initial} - S \quad \text{(A-13)}$$

$$[H_2O]_{eq} = [H_2O]_{initial} - S \quad \text{(A-14)}$$

$$[CO_2]_{eq} = [CO_2]_{initial} + S \quad \text{(A-15)}$$

$$[H_2]_{eq} = [H_2]_{initial} + S \quad \text{(A-16)}$$

Once the equilibrium composition is known, the fractions of H_2 and CO required to react with the O_2 are calculated by assuming that they are in the same ratio of their mole fractions at the time of reaction.

$$[H_2]_{Aft\_combst} = [H_2]_{eq}\left(1 - \frac{2J_{O_2}}{[H_2]_{eq} + [CO]_{eq}}\right) \quad \text{(A-17)}$$

$$[CO]_{Aft\_combst} = [CO]_{eq}\left(1 - \frac{2J_{O_2}}{[H_2]_{eq} + [CO]_{eq}}\right) \quad \text{(A-18)}$$

$$[H_2O]_{Aft\_combst} = [H_2O] + [H_2]_{eq}\frac{2.J_{O_2}}{[H_2]_{eq} + [CO]_{eq}} \quad \text{(A-19)}$$

$$[CO_2]_{Aft\_combst} = [CO_2] + [CO]_{eq}\frac{2.J_{O_2}}{[H_2]_{eq} + [CO]_{eq}} \quad \text{(A-20)}$$

Now, the next step is to calculate the exit stream compositions ($[H_2]_{ex}$, $[CO]_{ex}$, $[H_2O]_{ex}$, and $[CO_2]_{ex}$) in the same way as we calculated the equilibrated inlet stream composition using Equations (A-5) to (A-16).

Next, the average gas compositions on which the cell's performance will depend are calculated as the average of the inlet and exit equilibrated stream compositions:

$$[H_2]_{av} = [H_2]_{eq} + [H_2]_{ex} \quad \text{(A-21)}$$

$$[CO]_{av} = [CO]_{eq} + [CO]_{ex} \quad \text{(A-22)}$$

$$[H_2O]_{av} = [H_2O]_{eq} + [H_2O]_{ex} \quad \text{(A-23)}$$

$$[CO_2]_{av} = [CO_2]_{eq} + [CO_2]_{ex} \quad \text{(A-24)}$$

Now, we calculate the partial pressure of each of the species:

$$P_{H_2} = P_{in}\frac{[H_2]_{av}}{[H_2]_{av} + [CO]_{av} + [H_2O]_{av} + [CO_2]_{av}} \quad \text{(A-25)}$$

$$P_{CO} = P_{in}\frac{[CO]_{av}}{[H_2]_{av} + [CO]_{av} + [H_2O]_{av} + [CO_2]_{av}} \quad \text{(A-26)}$$

$$P_{H_2O} = P_{in}\frac{[H_2O]_{av}}{[H_2]_{av} + [CO]_{av} + [H_2O]_{av} + [CO_2]_{av}} \quad \text{(A-27)}$$

$$P_{CO_2} = P_{in}\frac{[CO_2]_{av}}{[H_2]_{av} + [CO]_{av} + [H_2O]_{av} + [CO_2]_{av}} \quad \text{(A-28)}$$

The next task is to calculate the average partial pressures of oxygen over the anode and cathode.

Cathode Side:

The partial pressure of the inlet stream is,

$$(PO_2)_{in} = P_{in}\frac{[O_2]_{in}}{Air_{in}} \tag{A-29}$$

From Equation A-1, the partial pressure of the outlet stream is given by,

$$(PO_2)_{out} = P_{in}\frac{[O_2]_{in} - J_{O_2}}{Air_{in}} \tag{A-30}$$

Using Equations A-29 and A-30, the average O_2 pressure on the cathode side can be found,

$$(PO_2)_{cathode} = \exp[\log(PO2)_{in} + \log(PO2)_{out}]/2 \tag{A-31}$$

Anode Side:

At the anode side, the partial pressures of oxygen at the inlet and outlet are found by assuming that the gaseous mixture remains in equilibrium:

Consider the combustion reaction:

$$H_2 + 1/2O_2 \leftrightarrow H_2O \tag{A-32}$$

At the inlet,

$$(PO_2)_{in} = \left[\frac{(PH_2O)_{in}}{\exp(K_{eq})\times(PH_2)_{in}}\right]^2 \tag{A-33}$$

similarly, at the exit,

$$(PO_2)_{out} = \left[\frac{(PH_2O)_{in}}{\exp(K_{eq})\times(PH_2)_{in}}\right]^2 \tag{A-34}$$

Now, using Equations A-33 and A-34, the average pressure of oxygen on the anode side,

$$(PO_2)_{anode} = exp[log(PO_2)_{in} + log(PO_2)_{out}]/2 \tag{A-35}$$

2. OPEN CIRCUIT VOLTAGE AND LOSSES

The open circuit voltage is calculated using the Nernst equation in the following manner:

$$V_{OC} = \frac{RT}{4F} Log\left(\frac{(PO_2)_{cathode}}{(PO_2)_{anode}} \right) \quad \text{(A-36)}$$

The operating voltage is obtained by subtracting the following irreversibilities:

1. Ohmic losses

The ohmic losses due to cell components are found by first calculating the area specific resistance (ASR) and then multiplying it by the current density.

$$ASR_j = \frac{I_j}{\sigma_j} \quad \text{(A-37)}$$

here, j refers to the j^{th} component of the cell, I_j is the thickness, and σ_j is the conductivity.
Hence, the voltage loss due to ohmic resistance is,

$$V_{ohmic} = i.ASR_j \quad \text{(A-38)}$$

where "*i"* is the current density.

- Resistive loss of cell components

Electrolyte: The electrolyte of the SOFC (YSZ) offers considerable resistance. The conductivity of YSZ is calculated by:

$$\sigma_{YSZ} = A.T^3 + B.T^2 + C.T + D \quad \text{(A-39)}$$

where the constants *A,B,C,* and *D* are empirically derived coefficients.

Electrodes: The electrodes of the fuel cell have relatively small resistance. Their effective conductivity depends upon the conductivity of the material (LSM 16 in the cathode and Ni-YSZ in the anode) and the porosity.

$$\sigma_{eff\ ,eletrode} = \sigma_{electrode}(1 - .V_{electrode}) \quad \text{(A-40)}$$

where $V_{electrode}$ is the porosity of the electrode.

$$\sigma_{cathode} = \frac{A}{T} \exp \frac{-E_{act}}{k.T} \quad \text{(A-41)}$$

where A is an empirically determined constant and E_{act} is the activation energy for the cathode material. σ_{anode} is assumed to be independent of temperature (conductivity of Ni-YSZ=1000 Ω / cm)

- Resistive loss of interconnect components and interfaces

***Interconnect*:** Stainless steel is used as interconnect,

$$\text{Conductivity, } \sigma_{ferric,SS} = \frac{1}{A.T + B} \qquad \text{(A-42)}$$

where A and B are empirically fitted constants.

Contact resistance: There is one additional ohmic loss associated with the contact resistance. It is treated as an adjustable parameter in the current modeling based upon empirical results.

2. Activation Losses

The activation loss is calculated using the Butler-Volmer equation. The data for temperature dependence at high fuel concentration was fitted by adjusting the Butler-Volmer parameters: the symmetry factor (α), the pressure-dependent pre-exponential term ($P_{\exp}$), and the activation energy for charge transfer (E_{act}).

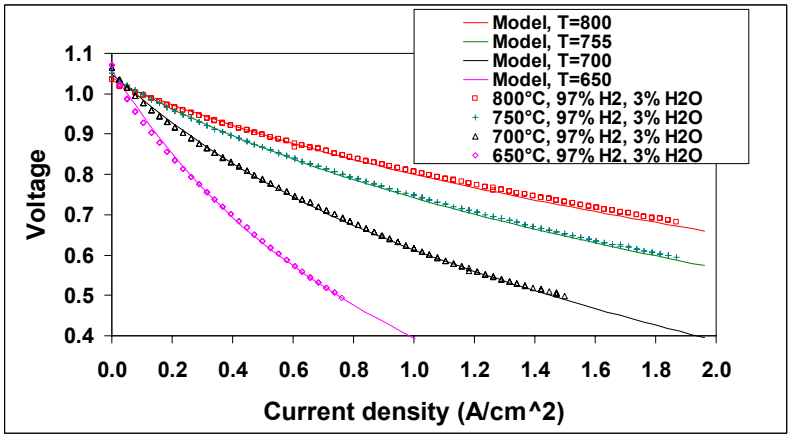

Figure A-2 SOFC Single Cell Voltage as Function of Current Density for a Range of Cell Operating Temperatures [PNNL, 2002]

$$\text{Butler-Volmer Voltage, } V_{B-V} = \frac{R.T}{\alpha.F}.Sinh^{-1}\left(\frac{i}{2.i_0}\right) \qquad \text{(A-43)}$$

and,

$$i_0 = P_{\exp}.\exp\left(\frac{-E_{act}}{R.T}\right) \qquad \text{(A-44)}$$

Where i_0 is the exchange current density, i is the average cell current density and α, $P_{\exp}$ and E_{act} are the adjustable parameters as discussed above.

3. Diffusion losses

As mentioned earlier, diffusion losses take place due to the depletion of fuel or oxygen at the electrode-electrolyte interface. Cathode diffusion losses do not dominate the diffusion and no discernable effect is generally seen until almost all the oxygen is exhausted. The modeling of oxygen diffusion through cathode is simple as there is only oxygen that is diffusing whereas in case of anode reactants ($H_2 + CO$) and products ($H_2O + CO_2$) both diffuse through, and modeling is rather difficult.

Cathode diffusion:

$$V_{cathode} = \frac{R.T}{4.F}.\log\left(\frac{1-i}{i_{cathode}}\right) \tag{A-45}$$

and,

$$i_{cathode} = \left(\frac{4.F.P.D_{eff,cathode}}{R.T.l_{cathode}}\right).\log\left(\frac{P}{P-P_{O_2}}\right) \tag{A-46}$$

where,

$D_{eff,cathode}$ - effective diffusion coefficient

P - system pressure

$l_{cathode}$ - cathode thickness

P_{O_2} - partial pressure of oxygen over cathode

The effective diffusion oxygen coefficient can be found if the binary diffusion coefficient of oxygen, the cathode porosity, and the tortuosity are known :

$$D_{eff,cathode} = D_{O_2-N_2}.\left(\frac{V_{cathode}}{\tau_{cathode}}\right) \tag{A-47}$$

and,

$$D_{O_2-N_2} = \left(\frac{T^{1.75}}{P}\right).\left(\frac{\sqrt{\frac{1}{M_{O_2}}+\frac{1}{M_{N_2}}}}{r_{O_2}+r_{N_2}}\right) \tag{A-48}$$

where,

M_{O_2} , M_{N_2} - molecular weight of oxygen and nitrogen respectively.

r_{O_2} , r_{N_2} - empirical molecular radius of oxygen and nitrogen.

Anode diffusion:

Two parallel reactions (A-49 and A-50) are occurring at the anode of the SOFC. The reactions are modeled using an electrical circuit analogy.

$$H_2 + 1/2O_2 \rightarrow H_2O \quad \text{(A-49)}$$

$$CO + 1/2O_2 \rightarrow CO_2 \quad \text{(A-50)}$$

Analogy:

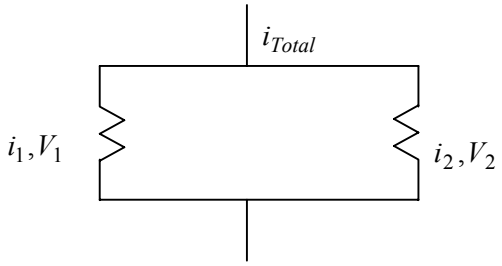

by Krichoff law,

$$i_1 + i_2 = i_{Total}, \quad V_1 = V_2 \quad \text{(A-51)}$$

where V_1 and V_2 and the overpotentials are calculated using the limiting current approach [Larmine, 2000]. Each branch contains a reactant (H_2 / CO) and a product (H_2O / CO_2).

$$V_{H_2} = \frac{RT}{2F}\left[\log\left(1 - \frac{i_1}{i_{H_2}}\right) + \log\left(1 - \frac{i_1}{i_{H_2O}}\right)\right] \quad \text{(A-52)}$$

$$V_{CO} = \frac{RT}{2F}\left[\log\left(1 - \frac{i_2}{i_{CO}}\right) + \log\left(1 - \frac{i_2}{i_{CO_2}}\right)\right] \quad \text{(A-53)}$$

where $i_{H_2}, i_{H_2O}, i_{CO}, i_{CO_2}$ are the limiting currents.

By solving Equations A-51, A-52, and A-53, the anode overpotential is written as a quadratic solution:

$$V_{anode} = \frac{R.T}{4.F}\log\left(\frac{-B + \sqrt{B^2 - 4.A.C}}{2.A}\right) \quad \text{(A-54)}$$

where,

$$A = \frac{i}{i_{H_2O}.i_{CO_2}} + \frac{1}{i_{H_2O}} + \frac{1}{i_{CO_2}} \quad \text{(A-55)}$$

$$B = \frac{i}{i_{H_2O}.i_{CO}} + \frac{1}{i_{H_2}.i_{CO_2}} + \frac{1}{i_{H_2}} + \frac{1}{i_{CO}} - \frac{1}{i_{H_2O}} - \frac{1}{i_{CO_2}} \quad \text{(A-56)}$$

$$C = \frac{i}{i_{H_2}.i_{CO}} - \frac{1}{i_{H_2}} - \frac{1}{i_{CO}} \quad \text{(A-57)}$$

now, the next step is to solve for the limiting currents. Limiting currents are derived for open circuit conditions and assume that the reactant concentrations approach zero in the gas immediately at the reaction sites. The limiting current is defined by the partial pressure, effective diffusivity (D^{eff}), and anode thickness (L_a) and it differs for reactants and products. The model assumes that except for H_2, the rest of the limiting currents are controlled by bulk diffusion through the pores:

$\phi = porosity$, $\tau = tortuosity$, $x = mole\ fraction$, $P = total\ pressure$, M=molecular weight, r=molecular radius

$$i_{H_2O} = \frac{2.F.P_{H_2O}.D^{eff}{}_{H_2O}}{R.T.L_a} \tag{A-58}$$

$$D^{eff}{}_{H_2O} = \frac{\phi.D^{uniary}{}_{H_2O}}{\tau} \tag{A-59}$$

$$D^{uniary}{}_{H_2O} = \frac{1 - x_{H_2O}}{\sum_{i \neq j} x_i / D^{binary}{}_{i,j}} \tag{A-60}$$

$$D^{binary}{}_{i,j} = \frac{.001.T^{1.75}\sqrt{\frac{1}{M_i} + \frac{1}{M_j}}}{P.\left(r_i + r_j\right)^2} \tag{A-61}$$

The model assumes that the concentration polarization due to limited reactant (H_2) supply rates is caused by the surface absorption and diffusion mechanisms very near to triple phase boundary (TPB), rather than by bulk diffusion mechanisms through the porous ceramic. The model describes how the concentration polarization is controlled by two localized phenomena: competitive adsorption of reactants in areas adjacent to the reactive TPB sites, followed by relatively slow surface diffusion to the reactive sites. Figure A-3 illustrates how faster bulk gas diffusion dominates at low current demand or high gas supply, while adsorption and slower surface diffusion dominate at high current demand or low gas supply. At low current densities, the reactants partial pressures are high near the TPB sites and diffusion can be considered as a combination of bulk and surface diffusion (Top diagram, Figure A-3). At low partial pressure of reactants caused by high current or high fuel utilization, the diffusion paths operate in series (Bottom diagram, Figure A-3).

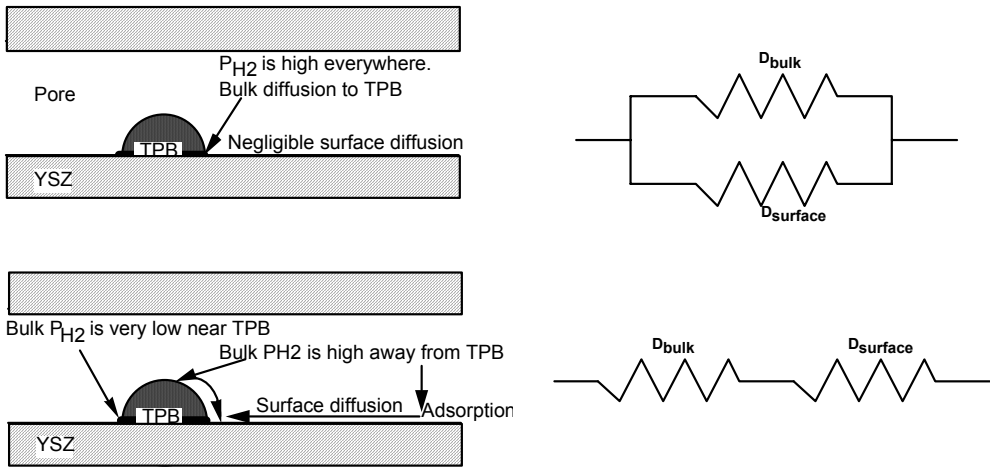

Figure A-3 Parallel Bulk Gas and Surface Diffusion at High Reactant pressure (top diagrams). The Series diffusion paths at Low Reactant Pressure (bottom diagrams) [Chick, 2003]

TPB's active reaction sites are occupied by H_2O at high temperature. H_2 absorbs on regions adjacent to the TPB and diffuses along the surface to the TPB. At the reaction sites, H_2 reacts and forms new H_2O and old H_2O desorbs (Figure A-4).

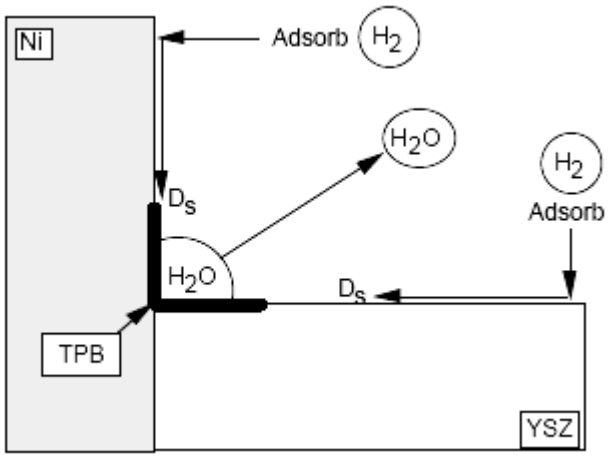

Figure A-4 Surface Absorption of H2 and Desorbtion of H2O Molecule [Chick, 2003]

The limiting current expression for H_2 is similar to Equation A-58, but the effective diffusion coefficient is calculated by Langmuir method. The effective diffusion coefficient is a combination of bulk diffusion coefficient and surface diffusion coefficient and the contribution of each is dependent on the surface coverage (monolayer absorption) of the gas which is found out by Langmuir's multi-gas isotherm [Chick, 2003]

Surface coverage of species *i*,

$$\theta_i = \frac{b_i P_i}{1 + \sum_j b_j P_j} \tag{A-62}$$

and,
$$b_i = \frac{N_A A_i \tau_0}{\sqrt{2\pi RTM_i}} e^{\frac{Q_i}{RT}} \tag{A-63}$$

where,

θ_i – surface coverage ($0 < \theta < 1$)
b_i – Langmuir parameter for species *i*
P_i - Partial pressure for species *i*
N_L - Avogadro number
A_i - area of the gas molecule on the surface
τ_0 - vibrational period
M_i - molecular weight
Q_i - absorption activation energy

now, the effective diffusion coefficient is given by:

$$D^{eff}{}_{H_2} = \left(D_{bulk}\right)^{\Theta} \left(D_{surf}\right)^{1-\Theta} \tag{A-64}$$

where D_{bulk} is the uniary gas diffusion coefficient for H_2 and can be calculated using Equation A-60 and A-61. D_{surf} is calculated as under:

$$D_{surf,H_2} = \frac{D^{1-\theta_i}{}_{surf,H_2,0} D^{\theta_i}{}_{surf,H_2,1}}{1-\theta_i} \tag{A-65}$$

for H_2 on nickel at ~1023K

$D_{surf,H_2,0} \sim 0.1 cm^2$ / sec at zero coverage

$D_{surf,H_2,1} \sim 5 \times 10^{-4} cm^2$ / sec at full coverage

Once we know all the limiting currents, they can be substituted into Equation A-54 and the diffusion loss can be calculated. This information together with the ohmic losses (A-38), and the activation losses (A-43), allow us to compute the net operating voltage,

$$V_{OP} = V_{OC} - V_{Ohmic} - V_{B-V} - V_{cathode} - V_{anode} \tag{A-66}$$

3. HEAT TRANSFER CALCULATIONS

Although, the heat transfer calculations in the extended stack model follow a different approach, the basic PNNL's unit button cell model's enthalpy calculations are presented for the sake of completeness. The following are the steps used to calculate the heat transfer in the button cell model:

Step 1:

First, the fuel gas mixture is virtually cooled down to room temperature and the enthalpy change is calculated for all the species (H_2, CO, H_2O, CO_2, N_2 if any):

$$\Delta H_i = \int_{T_{inlet}}^{T_{298}} Cp_i dT \tag{A-67}$$

Now,

$$\Delta H_{cooling} = \sum \Delta H_i \tag{A-68}$$

Step 2:

The appropriate amounts of H_2 and CO (based on inlet and outlet fuel concentrations) are oxidized at room temperature using room temperature enthalpies of formation for products and reactants.

$$CO + 1/2O_2 \rightarrow CO_2 \quad \Rightarrow \quad \Delta H_1 = \Delta H_f(CO) + \Delta H_f(CO_2) \tag{A-69}$$

$$H_2 + 1/2O_2 \rightarrow H_2O \quad \Rightarrow \quad \Delta H_2 = \Delta H_f(H_2O) \tag{A-70}$$

Now,

$$\Delta H_{OX} = \Delta H_1 + \Delta H_2 \tag{A-71}$$

Step 3:

The anode mixture is again heated to the to the outlet temperature.

$$\Delta H_i = \int_{T_{298}}^{T_{outlet}} Cp_i dT \tag{A-72}$$

and,

$$\Delta H_{heating} = \sum \Delta H_i \tag{A-73}$$

Step 4:

Now the net enthalpy change on the anode side is the sum of enthalpies due to cooling, oxidation and heating,

$$\Delta H_{net} = \Delta H_{cooling} + \Delta H_{OX} + \Delta H_{heating} \tag{A-74}$$

The heat produced due to the oxidation on the anode side of the cell is the difference between the change in enthalpy and the power produced by the cell,

$$Q_{OX} = \Delta H_{net} - Work_{Elec} \tag{A-75}$$

Step 5:

The changes in the enthalpy associated with the removal of heat by cathode air as it passes through the stack are calculated using the same methodology as for fuel cell oxidation.

$$\Delta H_i = \int_{T_{inlet}}^{T_{outlet}} Cp_i dT \tag{A-76}$$

where *'i'* is N_2 or O_2.

$$Q_{cath} = \Delta H_{cath} = \Delta H_{N_2} + \Delta H_{O_2} \tag{A-77}$$

Step 6:

Now the net heat generated in the cell is obtained by adding the enthalpy of fuel oxidation and the enthalpy of cathode air heating,

$$Q_{net} = Q_{ox} + Q_{cath} \tag{A-78}$$

It is important to note that the heat losses due to convection/radiation are ignored in the current modeling.

The above discussion completes the discussion of PNNL's unit button cell model. The results of the button cell model are discussed in the chapter presenting the results.

REFERENCES

[Angrist, 1965] Angrist, Stanley W., *Direct Energy Conversion,* Boston, Allyn and Bacon, 1965.

[Bejan, 1995] Bejan, Adrian, *Convection Heat Transfer,* Second Edition, Wiley, New York, 1995.

[Brinson, 2004] Brinson, Thomas, *Summer Internship Final Report,* NASA Glenn Research Center , Ohio, 2004.

[Campanari, 2000] Campanari, S., *Full load and part-load performance prediction for integrated SOFC and microturbine systems*, Journal of Engineering for Gas Turbines and Power, 2000, Vol. 122, p 239-246.

[CAPS, 2005] Freeh, Joshua E., *A Presentation on Solid Oxide Fuel Cell/Gas Turbine Hybrid Systems for Auxiliary Power,* Center for Advanced Power System, April 19, 2005.

[C-Doctors, 2006] http://www.corrosion-doctors.org/FuelCell/pafc.htm, visited on May 2, 2006.

[Chan, 2002] Chan, S. H., Ho, H. K., Tian, Y., *Modeling of simple hybrid solid oxide fuel and gas turbine power plant*, Journal of Power Sources, 109 (2002) 111-120.

[Chan, 2003] Chan, S. H., Ho, H. K., Tian, Y., *Multi-level modeling of SOFC-gas turbine hybrid system*, International Journal of Hydrogen Energy, 28 (2003) 889-900.

[Chick, 2003] Chick, Larry, Stevenson, Jeff, Williford Rick, *Spreadsheet Model of SOFC Electrochemical Performance,* Aug 29, 2003.

[Costamagna, 2001] Costamagna, P., Magistri, L., Massardo, A. F., *Design and part-load performance of a hybrid system based on a solid oxide fuel cell reactor and a micro gas turbine*, Journal of Power Sources, 96 (2001) 352-368

[Desideri, 2005] Desideri, Umberto, Lazaroiu, Gheorghe, Zaninelli Dario, Lazaroiu, Cristian, *A Matlab-Simulink Analysis of Hybrid SOFC Dynamic Behavior,* Third International Conference of Fuel Cell Science and Technology, May 23-25, 2005, FUELCELL2005-74056.

[Equest, 2006] *http://www.energyquest.ca.gov/time_machine/700000bce-1000bce.html*, visited on May 1, 2006.

[FCH, 2004] EG&G Technical Services, Inc, *Fuel Cell Handbook,* U.S. Department of Energy, National .Energy Technology Laboratory, West Virginia, Nov, 2004.

[FCtoday, 2006]

http://www.fuelcelltoday.com/FuelCellToday/EducationCentre/EducationCentreExternal/EduCentreDisplay/0,1741,History,00.html, visited on May 1, 2006.

[Freeh, 2005] Steffen, Christopher J., Jr., Freeh, Joshua E., Larosiliere, Louis M., *Solid OxideFuel Cell/Gas Turbine Hybrid Cycle Technology for Auxiliary Aerospace Power,* ASME TURBO EXPO 2005, GT2005-68619.

[Hermann, 2002] Hermann, F., Pålsson, J., Mauss, F., *Combustor Design Analysis for SOFC Off-gases.* Fifth European Solid Oxide Fuel Cell Forum, 1.-5. July 2002, Lucerne, Switzerland.

[Jenne, 2002] Jenne, M., Zähringer, T., *Sulzer Hexis SOFC systems for biogas and heating oil,* Proceedings of the 5th European Fuel Cell Forum, 1-5 July, 2002, Lucerne, Switzerland, Vol. 1, p 461-466.

[Kurzke, 2004] Kurzke, J., *Compressor and Turbine Maps for Gas Turbine Performance Computer Programs - Component Map Collection 2,* Joachim Kurzke, Dachau, 2004.

[Larminie, 2000] Larminie, J., Dicks, A., *Fuel Cell Systems Explained,* John Wiley & Sons Ltd., New York, 2000.

[Magistri, 2002] Magistri, L., Bozzo, R., Costamagna, P., Massardo, A. F., *Simplified versus detailed SOFC reactor models and influence on the simulation of the design point performance of hybrid systems,* ASME TURBU EXPO 2002, GT-2002-30653.

[Palsson, 2000] Palsson, J., Selimovic, A., Sjunnesson, L., *Combined solid oxide fuel cell and gas turbine systems for efficient power and heat generation*, Journal of Power Sources 86 (2000) 442-448.

[Palsson, 2002] Palsson, J., *Thermodynamic Modeling and Performance of Combined Solid Oxide Fuel Cell and Gas Turbine Systems,* Doctoral Thesis, Lund University, ISSN 0282-1990.

[PNNL, 2002] Chick, L., Stevenson, J., Williford, R., Simner, S.,Windisch, C.F., *Experimentally-Calibrated, Spread Sheet based SOFC Unit Button Cell Model, Revision 43a,*Pacific Northwest National Laboratory, Aug 29, 2002.

[Rao, 2001] Rao, A. D., Samuelsen, G. S., *A Thermodynamic analysis of tubular sofc based hybrid systems*, Proceedings of ASME TURBO EXPO 2001, 2001-GT-0522.

[Samuelsen, 2004] Samuelsen, *S., Turbo fuel cell report: Fuel Cell/Gas Turbine Hybrid Systems,* National Fuel Cell Research Center, University of California, Irvine, CA, Feb, 2004.

[Saunders, 2002] Saunders, G. J., Kendall, K., *Reactions of hydrocarbons in small tubular SOFCs,* Journal of Power Sources, Vol. 106, 2002, p 258-263.

[Selimovic, 2002] Selimovic, Azra, *Modeling of Solid Oxide Fuel Cells Applied to the Analysis of Integrated Systems with Gas turbines,* Doctoral Thesis, 2002, Lund University, Division of Thermal Power and Engineering, Department of Heat and Power Engineering.

[Steffen, 2005] Steffen, Christopher J., Jr., Freeh, Joshua E., Larosiliere, Louis M., *Off-Design Performance Analysis of a Solid Oxide Fuel Cell/Gas Turbine Hybrid for Auxiliary Aerospace Power,* Third International Conference of Fuel Cell *Science* and Technology, May 23-25, 2005, FUELCELL2005-74099.

[Thorud, 2005] Thorud, Bjorn, *Dynamic modeling and characterization of a Solid Oxide Fuel Cell Integrated in a Gas Turbine Cycle,* Doctoral Thesis, 2005, Norvegian University of Science and Technology, Department of ISSN 1503-8181

[Winkler, 2000] Winkler, W., Hagen, L., *Layout of SOFC-GT cycles with electric efficiencies over 80%,* Proceedings of the 4th European Fuel Cell Forum, 1-5 July, 2000, Lucerne, Switzerland, Vol. 1, p 413-420.

[Yi, 2004] Yi, Y., Rao, A. D., Brouwer, J., Samuelsen, S. G., *Analysis and optimization of a solid oxide fuel cell and intercooled gas turbine (SOFC-*ICGT) hybrid cycle, Journal of Power Sources, 134 (2004) 77-85.

BIOGRAPHICAL SKETCH

Nischal Srivastava was born on 11-07-1979 in Lucknow, India. After compleing his Bachelor's degree in Aerospace engineering from Indian Institute of Technology, Kanpur in 2001, he worked for a software company for almost 2 years in India. He joined Florida State University in spring, 2005 as a Master's student in Mechanical Engineering and completed the degree in summer, 2006.